Cavendish–HEP–95/18
DFTT 79/95
DTP/95/104
November 1996

Higgs Production at the LHC: an Updated Signal-to-Background Analysis

Stefano Moretti[1]

Cavendish Laboratory, University of Cambridge,
Madingley Road, Cambridge, CB3 0HE, United Kingdom.

Dipartimento di Fisica Teorica, Università di Torino,
and I.N.F.N., Sezione di Torino,
Via Pietro Giuria 1, 10125 Torino, Italy.

Abstract

This paper follows Ref. [1], where updated calculations of cross sections and branching ratios relevant for Standard Model Higgs phenomenology at the LHC were presented. Here, we complete that study by carrying out an updated signal-to-background analysis. We present results obtained by using exact matrix element computations at parton level for all processes, by exploiting the most recent parton distributions fitted to HERA structure function data and the most recent values of the electroweak input parameters. Cross sections and distributions are given for two collider energies, $\sqrt{s_{pp}} = 10$ TeV and 14 TeV. Event rates and significances are discussed for two possible values of integrated luminosity, 10 fb^{-1} and 100 fb^{-1}.

[1]E-mails: Moretti@hep.phy.cam.ac.uk.; Moretti@to.infn.it

1 Introduction

The search for the Standard Model ($\mathcal{SM}$) Higgs boson after LEP 2 and before a Next Linear Collider (NLC) relies on the Large Hadron Collider (LHC). The project of a proton-proton collider at CERN dates back to the end of the $Sp(\bar{p})S$ era, when the need of a hadron accelerator operating at the TeV scale in order to carefully study the Higgs sector of the $\mathcal{SM}$ clearly came out. At the beginning, the LHC was planned as a machine with a beam energy of 7.7 TeV and a design luminosity of 1.7×10^{34} cm^{-2} s^{-1} or more [2].

Since the time of the 1990 Large Hadron Collider Workshop [3], when all the most important physics issues which can be studied at the CERN pp accelerator were addressed in great detail (Higgs physics included), both the design of the machine and its foreseen performances have partially evolved. For example, the Centre-of-Mass (CM) energy has been reduced. In fact, the CERN Council finally decided in December 1994 that the LHC should be built as a two-stage project. The first stage being a particle collider with a CM energy of 10 TeV, which should be ready to start running in 2004. In 2008 the LHC should be upgraded by adding magnets to reach the final value $\sqrt{s}_{pp} = 14$ TeV. Not before 1997 it could be re-examined the two stage project, exploiting the possibility of reverting to the immediate construction of a 14 TeV accelerator to be ready by 2005. This however depends on the availability of sufficient financial commitments. In addition, the peak design luminosity has decreased as well, to 1.0×10^{34} cm^{-2} s^{-1} or a factor of ten less.

In the meanwhile, also the evolution of the LHC detectors has been greatly carried out, as new technologies have become available in the last six years. In particular, for what concerns Higgs physics, special attention has been devoted to the combined performances of: (i) the electromagnetic calorimeter and the inner detector, in view of higher mass resolutions in tagging $H \to ZZ^* \to 4e$ and $H \to \gamma\gamma$ signals, of more efficient γ/π^0 and γ/jet separation, and better b-tagging, especially using low p_T electrons; (ii) the muon chamber and the inner detector for studies of $H \to ZZ^* \to 4\mu$ with high mass resolution.

Recently, the Higgs discovery potential of the LHC has been carefully re-investigated in the Technical Proposals of the two experimental collaborations that will work at the CERN hadron collider: ATLAS [4] and CMS [5]. There, all the relevant information concerning the design/performances of the machine and of the detectors were also given. However, concerning the physics aspects of those analyses, a few important features must be noticed: first, predictions were given for the CM energy of 14 TeV only; furthermore, one often finds there slight inconsistencies in the way the signal and background rates were calculated and compared with each other (leading versus next-to-leading order cross sections, out-of-date parton distributions and parameter values, etc ...). Moreover, sometimes event rates were computed using exact matrix element calculations, whereas in other instances Monte Carlo event generators were used (such as, e.g., PYTHIA, HERWIG, GEANT [6]).

For this reasons, in Ref. [1], cross sections, branching ratios and event rates of signals relevant for Higgs phenomenology at the LHC were all recomputed. In that paper, all the most recent theoretical results and experimental inputs were included, such as:

(i) next-to-leading (NLO) order corrections to most of the Higgs production cross sections and partial decay widths;

(ii) new parton distribution functions, fitted to the high precision data mostly coming from deep inelastic scattering at HERA and to the latest measurements of α_s;

(iii) new input parameter values of physical quantities (in particular the top quark mass m_t), obtained from precision measurements performed at LEP, Tevatron and other machines.

The goal of the analysis carried out there was a set of benchmark results for cross sections and event rates as a function of M_H, for the two 'standard' LHC collision energies, $\sqrt{s}$ = 10 and 14 TeV. The predictions given in Ref. [1] enable the Higgs production and background rates as well as the significance factors used, e.g., in Refs. [4] and [5], to be normalised to the most up-to-date values.

This paper is, in a sense, the continuation of Ref. [1], as it contains an updated signal-to-noise analysis, which takes into account most of the theoretical improvements adopted in Ref. [1] as well as the new characteristics of the collider discussed above. However, as already mentioned in Ref. [1], we again stress here that we are not attempting to perform a detailed analysis of signals, backgrounds and search strategies: in this respect, by far the most complete studies to date can still be found in the ATLAS [4] and CMS [5] Technical Proposals. Instead, it is the purpose of the present study to approach the issue of phenomenological studies of Higgs signals and backgrounds at the LHC in the most coherent way, preferring *incompleteness* to *inconsistency*. In fact, throughout this paper, only *exact matrix element computations* are employed for *all processes*, both signal and background events, and no recourse to any Monte Carlo event generator is done. Not even fragmentation and hadronization phenomena are considered and no special effort in simulating detector effects (minimum bias events, smearing, pile-up, etc ...) is done either. All results are computed and cuts are applied at *parton level*. In evaluating the Feynman amplitude squared of the various processes, if not otherwise stated, we used the packages MadGraph [7] and HELAS [8] and the integrator VEGAS [9].

There is however a difference, with respect to Ref. [1]. As the most part of the backgrounds studied in literature have not benefited so far from much theoretical effort (contrary to the Higgs processes), such that most of them are known at tree–level only, we have adopted also for the signal rates the leading order (LO) results (contrary to Ref. [1]). Indeed, in the spirit of the approach we described, we have 'independently' computed here all background processes using perturbative techniques implementing standard Feynman rules.

Concerning the numerical part of our work, we have used for the electroweak and QCD input parameters the same values given in Ref. [1]. For reference we list them here too, they are:

$$\begin{aligned} M_Z &= 91.186 \text{ GeV}, & \Gamma_Z &= 2.495 \text{ GeV}, \\ M_W &= 80.356 \text{ GeV}, & \Gamma_W &= 2.088 \text{ GeV}, \\ G_F &= 1.16639 \times 10^{-5} \text{ GeV}^{-2}, & \alpha_{em} &\equiv \alpha_{em}(M_Z) = 1/128.9. \end{aligned} \tag{1}$$

The charged and neutral weak fermion–boson couplings are defined by

$$g_W^2 = \frac{e^2}{\sin^2\theta_W} = 4\sqrt{2}G_F M_W^2, \qquad g_Z^2 = \frac{e^2}{\sin^2\theta_W\ \cos^2\theta_W} = 4\sqrt{2}G_F M_Z^2. \tag{2}$$

For the vector and axial couplings of the Z boson to fermions, we use the 'effective leptonic' value $\sin^2_{\rm eff}(\theta_W) = 0.2320$. For the QCD strong coupling constant α_s we always adopt the expression at two-loops, with $\Lambda^{(4)}_{\overline{MS}} = 230$ MeV, in order to match our default parton distribution set MRS(A) [10], and with a scale μ set equal to the the subprocess invariant mass, $\mu = \sqrt{\hat{s}_{pp}}$. For the fermion masses we take $m_\mu = 0.105$ GeV,

$m_\tau = 1.78$ GeV, $m_s = 0.3$ GeV, $m_c = 1.4$ GeV, $m_b = 4.25$ GeV and $m_t = 175$ GeV [11, 12], with all decay widths equal to zero except for Γ_t. We calculate this at tree-level within the $\mathcal{SM}$, using the expressions given in Ref. [14]. The first generation of fermions and all neutrinos are taken to be massless, i.e. $m_u = m_d = m_e = m_{\nu_e} = 0$ and $m_{\nu_\mu} = m_{\nu_\tau} = 0$. Finally, we consider Higgs masses spanning in the range 80 GeV $\lesssim M_H \lesssim 700$ GeV, assuming that the first value is the (conservative) discovery limit for LEP2[2]. As usual, our discussion will be subdivided into two distinct classes, depending on whether M_H is less than (i.e., 'intermediate mass' range) or greater than (i.e., 'heavy mass' range) the WW-decay threshold around $2M_W$.

The plan of this paper is as follows. In Section 2 we review the most important Higgs signatures (see Ref. [1]) for a $\mathcal{SM}$ Higgs in the intermediate mass range. That is, we will proceed by studying the channels:

- $H \to \gamma\gamma$;
- $H \to b\bar{b}$;
- $H \to ZZ^* \to 4\ell$ ($\ell = e, \mu$);

and the corresponding backgrounds[3]. In Section 3 we concentrate on the heavy mass range, in particular, we will consider the following channels:

- $H \to ZZ \to 4\ell$ ($\ell = e, \mu$);
- $H \to ZZ \to \ell^+\ell^-\nu_{\ell'}\bar{\nu}_{\ell'}$ ($\ell = e, \mu$ and $\ell' = e, \mu, \tau$);

and again the corresponding backgrounds. Finally, in Section 4 we give a short summary and draw our conclusions.

[2]Note that the current lower limit on the Higgs mass from direct searches is 66 GeV [15], whereas from the fits to the LEP and SLD data one can deduce a 95% confidence level upper limit on M_H of 550 GeV (with the best χ^2 fit for $M_H = 149^{+148}_{-82}$ GeV) [16].

[3]Very recently (see Ref. [17]) it has been claimed that the decay $H \to W^{(*)}W^{(*)} \to \ell^+\nu_\ell\ell'^-\bar{\nu}_{\ell'}$, where $\ell, \ell' = e, \mu$, can give additional chances of Higgs detection in the window 155 GeV $\lesssim M_H \lesssim$ 180 GeV. In this case the lack of a measurable narrow resonant peak should be compensated by a relatively large branching ratio, since for the above mass range the WW-channel is the dominant decay mode.

2 The intermediate mass range

2.1 Search for $H \to \gamma\gamma$

The importance of the rare decay mode $H \to \gamma\gamma$ has been clearly explained in Ref. [1]. The highest rates for this channel occur in the region 80–150 GeV, where the combination of a rising branching ratio (see Fig. 1 in Ref. [1]) and a falling cross-section (see Figs. 5a–5b in Ref. [1]) yields rates which are remarkably constant over the above range. As it has been recently outlined that the region 80–100 GeV could be better probed by the channel $H \to b\bar{b}$, whereas for $M_H \gtrsim 130$ GeV the channel $H \to Z^*Z^* \to 4\ell$ becomes clearly visible, the two-photon decay should remain the best way to search for the Higgs boson in the mass interval 100–130 GeV [18].

It has been shown by ATLAS [4] that the potential interest of the inclusive channel $H \to \gamma\gamma$ (without isolated and high p_T leptons) would be limited to the region 80–100 GeV, and only after several years of data taking at high luminosity. However, since large part of this interval can be covered by LEP 2 (with $\sqrt{s}_{ee} \approx 200$ GeV) and/or Di–Tevatron (with $\sqrt{s}_{pp} \approx 4$ TeV), and since the bulk of the events at high significance would come anyway from the signature $\ell\gamma\gamma X$ (with an isolated high p_T lepton), we do not consider here this case. Somehow more optimistic prospects are given by CMS [5], which also considered the channel $H \to \gamma\gamma$ in association with high E_T/E jets.

We concentrate here on the associated production of the H with a $t\bar{t}$-pair or a W, followed by the (semi)leptonic decays $t\bar{t} \to \ell\bar{\nu}_\ell X$ and $W \to \ell\bar{\nu}_\ell$, respectively. These channels have substantially different characteristics with respect to the case of the direct $gg \to H \to \gamma\gamma$ production and decay. On the one hand, one has the disadvantage of production rates which are one order of magnitude smaller and a larger number of backgrounds (both reducible and irreducible). On the other hand, the primary vertex position can be more easily worked out, by using the charged lepton track [19] and, in addition, the isolated hard lepton from the W and t decays allows for a very strong reduction of the backgrounds. Finally, these advantages can be exploited both at high and low luminosity.

In order to account for the main features of the $WH \to \ell\gamma\gamma X$ and $t\bar{t}H \to \ell\gamma\gamma X$ signals, detectors must guarantee the following performances [5]:

- an electromagnetic calorimeter with excellent stability, uniformity and high energy and angular resolution, in order to extract the very narrow Higgs resonance in two photons from the continuum $\gamma\gamma$ background;

- a large acceptance;

- excellent neutral pions (giving photons) rejection, since QCD jets contain one or more leading π^0's (it has been estimated that a rejection factor $\gtrsim 5 \times 10^3 - 10^4$ should allow one to reduce the QCD backgrounds below the $\gamma\gamma$ continuum);

- powerful capability of the inner tracking system.

A very detailed description of the potential of the LHC detectors needed in order to make feasible to tag the Higgs boson in the di-photon channel can be found in Ref. [20]. Although this study dates back at the time of the first LHC Workshop (1990), nevertheless it still represents an excellent source of informations on this topic. We certainly refer the reader to that paper. In practice, what it is especially needed is that the LHC detectors can maintain an excellent photon energy and angular resolution, while the machine is running at full luminosity.

After applying standard acceptance cuts (see below), the main backgrounds to the $\ell\gamma\gamma$ Higgs signature via WH and $t\bar{t}H$ production have found to be the irreducible processes $W\gamma\gamma$ and $t\bar{t}\gamma\gamma$[4] and the reducible reactions $W\gamma j$ with the pions in the jet giving hard photons, $t\bar{t}\gamma$ with a jet and $Z\gamma$ with a $\ell^\pm$ from the Z-decay faking a photon, respectively. It has been shown in Ref. [5] that the processes Wjj and WZ as well as the channels $t\bar{t}\gamma j$, $b\bar{b}\gamma\gamma$, $c\bar{c}\gamma\gamma$, $b\bar{b}\gamma j$ and $c\bar{c}\gamma j$ give a minor contribution, so we dot treat them here.

The isolation criteria and cuts we have applied to select the signals are the same ones adopted by the CMS Collaboration in its Technical Proposal for the LHC [5]. We list them here for convenience:

- for photons, $|\eta^\gamma| < 2.4$, $p_T^{\gamma_1} > 40$ GeV, $p_T^{\gamma_2} > 20$ GeV;

- for leptons, $|\eta^\ell| < 2.4$, $p_T^\ell > 20$ GeV;

[4]In generating the results for the background $t\bar{t}\gamma\gamma$ we have used the code already employed in Ref. [21], for the subprocess $gg \to t\bar{t}\gamma\gamma$, whereas for the case $t\bar{t}\gamma$ it has been employed the program used in Ref. [22] (for both gg- and $q\bar{q}$-fusion).

- isolation of leptons and photons, i.e., no particles with $p_T > 2$ GeV in a azimuthal angle-(pseudo)rapidity cone of $\Delta R = \sqrt{\Delta\eta^2 + \Delta\phi^2}$,

where the subscripts 1 and 2 for the photons refer to the most and least energetic one, respectively. In the case of the background $Z\gamma$ the additional requirement $|M_Z - M_{\ell\gamma}| > 5$ GeV was also applied.

Figs. 1a–2a show the differential distribution of the sum of the signals and of the backgrounds, respectively, in the invariant mass $M_{\gamma\gamma}$, for $\sqrt{s}_{pp} = 10, 14$ TeV and $m_t = 175$ GeV. We have collected the signal rates in bins of 2 GeV around the Higgs mass (shown for the values 80, 100 and 120 GeV), as the Higgs resonance in this region is very narrow (e.g., $\Gamma_H \lesssim 0.01$ GeV). In the plots all the above cuts have been applied. They also include the suppression factor against π^0's in jets faking photons[5] and the fact that only 1% of the leptons from the Z decay in $WZ \to W\ell^+\ell^-$ are recognised as photons [4, 5] (the factor ε in the figures gives account of this). We have not considered the conversion loss, of $\mathcal{O}(10\% - 20\%)$ approximately, for tagging real photons [4, 5].

In Tab. I we have collected the number of signal S and background B events in a window of $\Delta M \equiv |M_H - M_{\gamma\gamma}| = 1$ GeV around the actual values of M_H, for the integrated luminosity $\mathcal{L} = 100$ fb^{-1}. Significances $S/\sqrt{B}$ are given for ΔM equal to 1, 2 and 3 GeV.

At $\sqrt{s}_{pp} = 10$ TeV, values of $S/\sqrt{B}$ are such that in the case the high luminosity option and good resolution in $M_{\gamma\gamma}$ can be contemporaneously guaranteed, i.e., $\mathcal{L} = 100$ fb^{-1} and $\Delta M \lesssim 3$ GeV, then Higgs detection should be promptly feasible for values of M_H in the range 80–120 GeV. Clearly, if the high luminosity option and/or high mass resolutions will not be possible, for $\sqrt{s}_{pp} = 10$ TeV, such chances would sensibly decrease (for example, for $\mathcal{L} = 10$ fb^{-1}, the significances in Tab. I are reduced by a factor $\sqrt{10} \approx 3.2$). This is particularly true for a light Higgs.

At $\sqrt{s}_{pp} = 14$ TeV values of $S/\sqrt{B}$ are larger by a factor of 1.3–1.4, if compared to those at 10 TeV, independently of M_H and m_t. This guarantees further possibilities of Higgs discovery, since even for very modest resolutions in $M_{\gamma\gamma}$ (although CMS claims that the mass resolution achievable could vary between 0.8 and 1.1 GeV [5] !) and/or a reduced luminosity, only the case $M_H \approx 80$ GeV would present some difficulties.

The relative contribution of the various background sources (before including any

[5]Which is equal to ≈ 5000 for $W\gamma$j and $t\bar{t}\gamma$ events, see Ref. [20] and also Ref. [4].

efficiency ε) can be appreciated in Figs. 1b and 2b (for $\sqrt{s}_{pp} = 10$ and 14, respectively).

2.2 Search for $H \to b\bar{b}$

An alternative strategy in searching for the $\mathcal{SM}$ Higgs boson in the intermediate mass range is to look for its main decay channel $H \to b\bar{b}$, by resorting to techniques of b-flavour identification [24, 25], thus reducing the enormous QCD backgrounds of light quark and gluon jets. This channel is the dominant decay mode in the range 80 GeV $\lesssim M_H \lesssim$ 130 GeV (see Fig. 1 of Ref. [1]). Around $M_H = 130$ GeV the decay $H \to WW^*$ starts dominating. The possibility of selecting the $b\bar{b}$ channel out of the huge QCD background by using the b–tagging capabilities of vertex detectors was first suggested in some theoretical papers [26, 27]. The main difficulties in this kind of search are the expected low Higgs rates after signal reconstruction, the necessity of gaining an accurate control of all the numerous background sources and the one of achieving very high b–tagging performances [18].

The chances to tag the $\mathcal{SM}$ Higgs boson via its main decay channel in the intermediate mass range are provided by the associate production mechanisms WH and $t\bar{t}H$, with the W and one of the top quarks decaying semileptonically to electrons or muons. The lepton is usually at high p_T and isolated, such that it can be used for triggering purposes. The expected signatures would then be $\ell b\bar{b}X$ (from WH) and $\ell b\bar{b}b\bar{b}X$ (from $t\bar{t}H$). Higgs signals in the $b\bar{b}$ channel would appear as a (narrow) peak in the invariant mass distribution of b-quark pairs.

In addition to the associated production with a charged vector boson and a $t\bar{t}$ pair, also other $\mathcal{SM}$ production mechanisms and signatures involving the decay $H \to b\bar{b}$ have been suggested in literature. We list them below for completeness although we will not treat them here, for the reasons that we are going to illustrate.

- ZH production [28] followed by the decays $Z \to \ell^+\ell^-$ ($\ell = e, \mu$) and $H \to b\bar{b}$. The disadvantages of this case are that, on the one hand, the production cross section is approximately six times lower that in the case of WH production whereas, on the other hand, the irreducible background $Zb\bar{b}$ is only ≈ 1.8 times smaller than the corresponding $Wb\bar{b}$ background to WH production.

- ZH production [28] followed by the decays $Z \to \nu\bar{\nu}$ and $H \to b\bar{b}$, as suggested in Ref. [26] (in the second paper). In this case it is very hard matter to reconstruct the final state [4], because of the presence of two neutrinos escaping the detectors. In addition, background processes with E_T^{miss} are large, if compared to the (rather low) signal.

Like in the case of the decay $H \to \gamma\gamma$, the challenge of the LHC in selecting the signature $H \to b\bar{b}$ requires very high performances from the detectors. Here we list the set of cuts we have adopted, which are the same ones used in Ref. [26] (and also, for comparison, in Ref. [18])[6].

- For the triggered lepton ℓ we require transverse momentum $p_T^\ell > 20$ GeV, pseudorapidity $|\eta^\ell| < 2.5$, and isolation from b-jets or partons $\Delta R_{b-jet,\ell} > 0.7$.

- Acceptance of events requires these to contain exactly two b-jets (or partons) with $p_T^{b-jet} > 15$ GeV, pseudorapidity $|\eta^{b-jet}| < 2.0$, and separation $\Delta R_{b-jet,b-jet} > 0.7$.

- Moreover, events are accepted if they do not contain any additional jet with $p_T^j > 30$ GeV and no more than one additional jet with $p_T^j > 15$ GeV, all of them with $|\eta^j| < 4.0$.

We first study the WH case, for which we assume the b-tagging efficiency to be $\epsilon_b = 50\%$ (for one b) whereas the rejection factor against non-b jets is taken to be $R = 50$ (the combination that seems to give higher significances [18]). The backgrounds to the channel $WH \to \ell b\bar{b}X$ that we have considered here are: WZ, $Wb\bar{b}$, $q\bar{q}' \to t\bar{b}$, $t\bar{t}$, $qg \to t\bar{b}q'$, Wjb and Wjj (see Ref. [26]). The dominant irreducible backgrounds are $Wb\bar{b}$ and, especially for M_H near M_Z, WZ with $Z \to b\bar{b}$. The dominant reducible noise comes from Wjj production, via Wgg, Wgq and $Wq\bar{q}$ partonic events[7], in which the two jets are misidentified as b-quarks, and Wjb (via the partonic production Wqb), for which this happens for one jet only. Top-antitop production and decay $t\bar{t} \to b\bar{b}W^+W^-$ with one W missed is another source of $\ell b\bar{b}X$ (reducible) events. Its control requires coverage of leptons to small p_T and of jets to high rapidity (see cuts discussed above): this in order to reduce the probability of missing a W. Moreover, in order to recognize such kind of events one can look for a W via the observation of an additional charged lepton,

[6]Apart from the cut on the missing transverse momentum (as $W \to \ell\nu$) $\not{p}_T > 20$ GeV, which has not been applied here.

[7]We checked that our codes reproduce the numbers given in Ref. [23].

of a jet with $p_T > 30$ GeV or of two jets with $p_T > 15$ GeV [26]. Pair production is not the only source of top quarks at the LHC. Other important reactions that constitute a background to WH are via the single top production: i.e., Wg fusion (where the 'initial' W is radiated off an incoming line of quarks), which gives the final state $tbq \to b\bar{b}qX$, and electroweak fusion (into a W) of a $q\bar{q}'$-pair. Whereas the former is a reducible background the latter is an irreducible one (as after top decay it yields the final state $Wb\bar{b}$ with no additional particle). In the first case, one can reject background events by asking that the additional jet from the outgoing quark has p_T less than 30 GeV.

Figs. 3a–4a show the differential distributions of the signal and of the sum of the various background components in the invariant mass $M_{b\bar{b}}$. We have collected the events rates in bin of 10 GeV around the Higgs mass (shown for 80, 100 and 120 GeV), at the values of CM energy of $\sqrt{s_{pp}} = 10$ and 14 TeV, respectively, with $m_t = 175$ GeV. The factor ε indicates that the above mentioned b-tagging performances are included. Tab. II collects the event rates for all the combinations of M_H and $\sqrt{s_{pp}}$, in a window of 30 GeV [26] around the Higgs masses, for 10 inverse femtobarns of integrated luminosity. Figs. 3b and 4b show the various background contributions separately (without any efficiency and/or rejection factor included).

By looking at Tab. II one can notice how significances are practically the same at both the energies 10 and 14 TeV, whereas signal rates differ, in general, by $\approx 35\%$. Chances of Higgs detection are larger for a light Higgs, as space phase effects are important. This situation is the opposite with respect to the channel $H \to \gamma\gamma$, where the significance of the signal grows with the increase of the Higgs mass (see Tab. I). Therefore, the $H \to b\bar{b}$ and $H \to \gamma\gamma$ channels seem to obey a sort of complementarity, for which the former might be the best way to probe the Higgs mass region 80 GeV $\lesssim M_H \lesssim$ 100 GeV, whereas the latter is better (at high luminosity) for 100 GeV $\lesssim M_H \lesssim$ 130 GeV. Therefore, our results qualitatively agree with those given in Ref. [18]. As clearly explained there, however, one has to remember that the quality of the Higgs signal extraction depends less crucially on the luminosity and on the detector performances in the second case. We refer the reader to Ref. [18] for a fuller discussion about this point.

In addition to the associated production with a W, also the $q\bar{q}, gg \to t\bar{t}H$ mechanism has been proposed as a viable channel to search for $H \to b\bar{b}$ decays [24], with the $t\bar{t}$-pair decaying inclusively to $\ell\nu_\ell X$ ($\ell = e, \mu$, as usual). Its production cross section for an intermediate mass Higgs and $m_t \approx 175$ GeV is of the same order as the WH one (even bigger for a heavier Higgs), see Figs. 5 and 6 of Ref. [1]. However, the corresponding final state is very complicated, since it consists of four b-quarks: $t\bar{t}H \to b\bar{b}b\bar{b}\ell\nu_\ell X$. The signal would appear as a peak in the invariant mass $M_{b\bar{b}}$, above the combinatorial background due to the signal itself and above the proper background processes. Clearly, the possibilities of disentangling the signal in this channel depend on the b-tagging performances of the LHC detectors even more than in the WH case. In particular, it has been shown that a high efficiency of b-tagging is more important than a large rejection of non-b jets [18].

We concentrate here on the search strategy that selects three b-quarks out of the four in the final state, as in general (except for values of ϵ_b much greater than 50%) the signal rates for four tagged b-jets are too low [18]. The backgrounds to the signature $b\bar{b}bWX$ (where the second b can be either a quark or an antiquark) in the region 80 GeV $\lesssim M_H \lesssim$ 140 GeV are given by the final states $t\bar{t}Z$ (which is irreducible), $t\bar{t}$, $t\bar{t}j$, $Wjjj$ and $t\bar{b}q$ production[8] (which are reducible) [4, 18].

The acceptance cuts we applied are the same of the WH case (for three b's/jets now and apart from the requirement $p_T^j > 30$ GeV on the q-jet of the $t\bar{b}q$ process, which has now been dropped). Also the selection of Higgs masses we considered here is the same, i.e., $M_H = 80, 100$ and 120 GeV. Numbers are given in Tab. III for two combinations of ϵ_b and R and for $\sqrt{s_{pp}} = 10$ and 14 TeV. The combined probability of picking three b's out of four in the case of the signal is here included.

In the case of $t\bar{t}H$ production, with respect to the case of WH associated production, the chances of Higgs detection via the $b\bar{b}$ decay channel are largely reduced (compare the significances in Tabs. II and III). The situation is slightly more optimistic at 14 TeV than at 10 TeV, as at lower energy the number of Higgs events is reduced by approximately a factor of two, making the low signal rates a serious problem. Significances are also generally larger for lighter Higgs masses. Notice however that these are the same characteristics of the $H \to b\bar{b}$ signal via WH production. Therefore, even though the $t\bar{t}H$ channel could not probably constitute a serious candidate to Higgs discovery on its own, nevertheless, if considered together with the WH channel, it should enhance the number of Higgs signals. In addition, the irreducible background in $t\bar{t}Z$ events is here quite small with respect to the signal $t\bar{t}H$, in the region $M_H \approx M_Z$, whereas this is not the case for WZ and WH [18]. Therefore, if the Higgs mass was 'around' the

[8] The background $q\bar{q}, gg \to t\bar{t}Z$ has been simulated by using the FORTRAN code adopted in Ref. [22].

Z-pole, the combination $WH + t\bar{t}H$ in the channel $H \to b\bar{b}$ should allow for Higgs detection, provided that a high b-tagging efficiency can be achieved, in order to remove the reducible background due to $Z \to jj$ decays [4, 18].

2.3 Search for $H \to ZZ^* \to 4\ell$

The four-lepton channel $H \to Z^{(*)}Z^{(*)} \to 4\ell$ with $\ell = e$ or μ (i.e., $H \to e^+e^-e^+e^- + \mu^+\mu^-\mu^+\mu^-$)[9] provides the best chances for Higgs detection over a substantially large portion of the Higgs mass range, between ≈ 130 and 800 GeV. Because of this and because its signature is relatively clean (especially if compared to the difficulties encountered for the $H \to \gamma\gamma$ and $H \to b\bar{b}$ cases), it is often nicknamed the 'gold-plated channel'.

If 130 GeV $\lesssim M_H \lesssim 2M_Z$, when one of the two Z-boson is off-shell (i.e., $H \to ZZ^*$), event rates are generally small (because of the still suppressed BR into the vector-pair) and the backgrounds can be dangerous (since the constraint $M_{\ell^+\ell^-} \approx M_Z$ can be applied to only one of the lepton pairs). However, in this mass range the Higgs width is still quite small (i.e., $\Gamma_H \ll 1$ GeV), therefore, provided that high enough lepton energy/angle resolution can be achieved, a substantial reduction factor on the background should be possible (in fact, the rates for the latter are directly proportional to the resolution itself). Also geometric and kinematical acceptances for leptons are crucial in this case [30].

In the mass region $M_H \lesssim 2M_Z$ the main backgrounds to the four-lepton signal of the $\mathcal{SM}$ Higgs boson come from $t\bar{t} \to b\bar{b}W^+W^-$, $Zb\bar{b}$ and ZZ^* production. In the first two backgrounds two of the leptons come from semi-leptonic b-decays, whereas the remaining two from the decays of the massive vector bosons (i.e., $W^+W^- \to \ell^+\ell^-X$ and $Z \to \ell^+\ell^-$). We approximated the semileptonic branching fraction of the b-quark, i.e., $BR(b \to \ell\nu X)$ where ℓ indicates a generic lepton, via the the one into c-quarks only (neglecting then the contribution coming from the decay $b \to u\ell\bar{\nu}_\ell$), since the ratio between the Cabibbo-Kobayashi-Maskawa coefficients entering in the two decays is $|V_{ub}/V_{cb}| = 0.10 \pm 0.03$ [2]. In computing the semileptonic BR of the b into c-quarks

[9] For simplicity we neglect here the mixed case $H \to e^+e^-\mu^+\mu^-$. However, its inclusion in the simulation would not change the main conclusions obtained in the case of identical leptons [29].

we have used the formula [2]

$$BR(b \to c\ell\bar{\nu}_\ell) = \Gamma(b \to c\ell\bar{\nu}_\ell)\tau_b = \frac{G_F^2 m_b^5}{192\pi^3}\beta(m_c, m_b)|V_{cb}|^2\tau_b, \tag{3}$$

where $\Gamma(b \to c\ell\bar{\nu}_\ell)$ is the partial width, τ_b the b-lifetime (≈ 1.3 ps, from the average over B hadrons) and $\beta(m_c, m_b) = \sqrt{1 - \frac{4m_c^2}{m_b^2}}$ the phase space factor, with $|V_{cb}| = 0.043 \pm 0.007$ [2] (the values for G_F, m_c and m_b were given previously). Therefore, the numerical value of $BR(b \to c\ell\bar{\nu}_\ell)$ is approximately 9%. As ZZ^* is an intermediate stage of the production and decay chain $H \to ZZ^* \to 4\ell$, the third background is irreducible.

Signal rates have been generated by using the mechanisms of gluon-gluon and vector-vector fusion production only [31], as $t\bar{t}H$ and WH/ZH are generally one order of magnitude smaller in the considered mass interval. As usual, signals and backgrounds have been generated using exact tree-level matrix element computations[10], apart from the subprocess $gg \to ZZ^*$ (through a higher order loop of quarks) that has not been calculated yet and that we have simulated by multiplying the $q\bar{q} \to ZZ^*$ rates by a factor 1.3 [33].

The strategy usually adopted in order to select the four-leptons events $H \to ZZ^*$ out of the above backgrounds is the following. In the case $\ell = e$, one requires:

- the most energetic electron must have $p_T^{e_1} > 20$ GeV, the second one $p_T^{e_2} > 15$ GeV, whereas for the remaining two the transverse momentum must be greater than 5 GeV for both. The rapidity of all four must be less than 2.5 (in absolute value).

In the case $\ell = \mu$, requirements are of the same type:

- the most energetic muon with $p_T^{\mu_1} > 20$ GeV, the second one with $p_T^{\mu_2} > 10$ GeV, whereas the remaining two μ's must have $p_T^{\mu_{3,4}} > 5$ GeV, all in the rapidity range $|\eta^\mu| < 2.4$.

In both cases $\ell = e$ and $\ell = \mu$ the invariant mass cut

- $|M_{\ell^+\ell^-} - M_Z| < 10$ GeV is finally applied.

[10] We have checked that our results reproduce those obtained in Ref. [32] for the subprocess $gg \to Zb\bar{b}$, initiated by gluon-gluon fusion. In the simulations, we have used the code already employed for the paper Ref. [22] (which includes also $q\bar{q}$-initiated subprocesses).

We notice that the latter constraint is extremely successful in rejecting the huge background coming from $t\bar{t}$ production, whereas it does not act on $Zb\bar{b}$ and ZZ^* production. However, the rates of the latter two processes are largely reduced by the separation criteria. For additional background suppression we in fact required (see [5]) isolation on any three of the four leptons, such that

- there is no track with $p_T^\ell > 2.5$ GeV within a ΔR cone of radius 0.2 around the lepton direction.

Our numerical results are given in Tab. IV for the channel $4\ell X$ and in Tab. V for the case $4\mu X$, where the number of signal (S) and background (B) events is presented, together with the corresponding significances ($S/\sqrt{B}$), for the value of integrated luminosity $\mathcal{L} = 100$ fb^{-1}. We show results for the selection of Higgs masses $M_H = 130, 150$ and 170 GeV. Significances are given for a window of 2, 4 and 6 GeV around M_H, the latter two in round and squared brackets, respectively.

The behaviour of the signal cross sections (in both channels $4\ell X$ and $4\mu X$) strongly reflects the characteristics of the branching ratio of the Higgs into two Z-bosons (see Fig. 1 in Ref. [1]). In fact, the highest rates occur for $M_H = 150$ GeV, value that corresponds to the local maximum in the $BR(H \to ZZ^*)$, whereas smaller rates occur for $M_H = 130$ and 170 GeV, the latter value corresponding to the local minimum in the ZZ-branching ratio (due to the opening of the real WW-threshold). We verified that the dependence on m_t for the signal is very weak (see also Figs. 5a–b), such that the total significances are practically unaffected by changes in m_t (we varied the top mass in the $t\bar{t}$ background accordingly).

Figs. 5–8 show the distribution in the invariant mass of the 4 leptons/muons. They give account also of the shape of the background. This is dominated by the $t\bar{t}$ component in the region $M_{4\ell,4\mu} \approx 130$ GeV, whereas the local maximum around $M_{4\ell,4\mu} = 190$ GeV is due to the opening of the threshold for the production of two real Z's in the background $pp \to ZZ$. The background from $pp \to Zb\bar{b}$ is never dominant (see also [4, 5]).

For the case of the $4\ell X$ channel, if the high luminosity option can be achieved, it should be possible to observe the Higgs boson in the intermediate mass range after one year or so of running, for all combinations of M_H and $\sqrt{s}_{pp}$. Particularly favourable is the case of $M_H = 150$ GeV, which should be resolved even for 10 fb^{-1}, both at 10 and 14 TeV of CM energy. For the lower luminosity option the case $M_H = 170$ GeV would present problems, independently of the mass resolution that could be achieved, whereas for $M_H = 130$ GeV, this happens if $\Delta M \gtrsim 2$ GeV, especially at 10 TeV.

The four muon case reflects more o less the same characteristics of the total 4ℓ case. Rates are obviously smaller than in the $4e + 4\mu$ case, however, acceptance criteria generally favour muon cross sections more than electron ones, both for signals and backgrounds. But whereas for the signal this happens with differences of just a few percents, in the case of the backgrounds the muon decays of the top quarks (after the above cuts) are about 40% larger than those into electrons, at fixed $\sqrt{s}_{pp}$ and m_t. Since top production is in general the dominant background, the final significances for the muon case are typically smaller than the ones of the 4ℓ case. Therefore, even more in this case, at low luminosity, Higgs with masses far away from the local maximum in the $BR(H \to ZZ^*)$ at $M_H = 150$ GeV, such as at 130 and 170 GeV, would be overwhelmed by the background, unless a really good muon resolution can be achieved (the latter is in fact the chance that induces to consider the four muon decay separately). For the case $M_H \approx 170$ GeV, the recourse to the channel $H \to W^{(*)}W^{(*)} \to \ell^+\nu_\ell \ell'^- \bar{\nu}_{\ell'}$, advocated in Ref. [17], might then be providential.

We would like here to conclude this subsection by stressing the importance of the isolation cut on three of the leptons, as this can greatly reduce the $t\bar{t}$ background (of a factor ≈ 5) and the $Zb\bar{b}$ one (of a factor ≈ 2). At the same time almost 95% of the $4e$ and 4μ signals pass this cut.

3 The heavy mass range

3.1 Search for $H \to ZZ \to 4\ell$, with $\ell = e$ or μ

In the case of heavy Higgs mass, when the on-shell decay $H \to ZZ$ can take place, the only significant background (after applying the invariant mass cut $M_{\ell^+\ell^-} \approx M_Z$ on both the lepton-antilepton pairs) is the continuum ZZ [4, 5]. Therefore, we concentrate on this background only. Here, p_T and η selection cuts on the four ℓ's are the same as in the ZZ^* channel for an intermediate mass Higgs. The sole difference is that in the heavy mass range we drop the requirement of isolation on three leptons, as it was previously implemented in view of reducing the $t\bar{t}$ background, which is here negligible compared to the ZZ contribution.

The invariant mass $M_{4\ell}$ for signal and background is shown in Figs. 9–10, for a CM energy of 10 and 14 TeV, respectively. The values for M_H here considered are 300, 500 and 700 GeV. In particular, Figs. 9a and 10a clearly show the feasibility of Higgs detection for a mass around 300 GeV, both at 10 and 14 TeV. For example, the number of signal and background events, for $\mathcal{L} = 100$ fb^{-1}, at $\sqrt{s}_{pp} = 10(14)$ TeV, is 214(408) and 123(102), respectively, in a 70 GeV window around the Higgs peak (i.e., $|M_H - M_{4\ell}| < 35$ GeV, since the total Higgs width for $M_H = 300$ GeV is equal to ≈ 8.4 GeV). Even the case of low luminosity (i.e., $\mathcal{L} = 10$ fb^{-1}) should allow one to reveal the Higgs scalar, after only one year of running. Higgs signals would appear as a broad Breit-Wigner resonance on top of a decreasing background (with increasing M_H), which has a maximum at $M_{4\ell} = 2M_Z$. The case of a Higgs scalar with mass around 500 GeV also allows for Higgs detection, as can be seen by looking at Figs. 9b and 10b.

Things are more complicated when one considers larger Higgs masses, like for example $M_H = 700$ GeV (Figs. 9c–10c). For such a value one looses the concept of resonance, as the Higgs particle has a width comparable to its mass, i.e., $\Gamma_H \approx 187$ GeV, and the characteristic Breit-Wigner peak disappears. In this case the shapes of signal and backgrounds are no longer easily distinguishable, and one has to be extremely careful in normalising the distributions. For the first stage energy $\sqrt{s}_{pp} = 10$ GeV, signal and background are hard to recognize (see Fig. 9c). At $\sqrt{s}_{pp} = 14$ TeV prospects are more optimistic, as here the maximum of the Higgs distribution at 700 GeV is a factor of three over the ZZ background (see Fig. 10c). In general, at higher CM energy, Higgs detection should then be feasible both at low and high collider luminosity.

3.2 Search for $H \to ZZ \to \ell^+\ell^-\nu_{\ell'}\bar{\nu}_{\ell'}$ ($\ell = e, \mu$ and $\ell' = e, \mu, \tau$)

The advantage of the $H \to \ell^+\ell^-\nu_{\ell'}\bar{\nu}_{\ell'}$ decay channel with respect to $H \to 4\ell$ is that it has a BR which is six times larger. The disadvantage is that, because of the presence of two neutrinos in the final state, invariant mass peaks around the actual Higgs mass value cannot be reconstructed. Therefore, this channel prevents from accurate studies of the Higgs parameters: e.g., the width Γ_H. The distinctive signature is two high p_T leptons (from one Z-decay) and high missing (transverse) energy E_T^{miss} (from the other

Z). The main backgrounds to the two-lepton-two-neutrino channel are the continuum production of two massive vector bosons (WZ and ZZ) plus the top-antitop production ($t\bar{t}$) and Z + jets. After the event selection cuts, the dominant background to the signal is the irreducible one $pp \to ZZ$, whereas the other three give smaller contributions [34, 35].

For $M_H \gtrsim 500$ GeV Higgs signals appear as broad Jacobian peaks in the two-lepton transverse momentum distribution. To select them we adopt the following procedure [5]. We require:

- $E_T^{miss} > 100$ GeV (which strongly suppresses the $Z+$ jets background)[11];
- $p_T^\ell > 20$ GeV, $|\eta^\ell| < 1.8$ and $p_T^{\ell\ell} > 60$ GeV;
- $|M_{\ell^+\ell^-} - M_Z| \leq 6$ GeV (which strongly reduces the reducible backgrounds);
- no jet with $E_T^j > 150$ GeV within $|\eta^j| \geq 1.8$;
- no back-to-back jets with the leptons (i.e., the cosine of the angle between the momentum of the jets and of $\ell^+\ell^-$ should be greater than -0.8).

Figs. 11 and 12 show the distribution on the transverse momentum of the lepton pair $\ell^+\ell^-$, after all cuts, for $M_H = 500$ GeV, at $\sqrt{s}_{pp} = 10$ and 14 TeV, respectively, for signal and background. The dependence on the collider CM is such that at 14 TeV one gets significances which are a factor 1.5 greater than at 10 TeV, with the number of events doubled. Assuming an integrated luminosity of 10 fb^{-1}, one obtains (in the window, say, $|p_T^{\ell\ell} - 225 \text{ GeV}| \leq 25$ GeV) 31.7(12.6) signal(background) events at 10 TeV. The corresponding numbers at $\sqrt{s}_{pp} = 14$ TeV are 67.6(19.4). Note that, in order to suppress the $t\bar{t}$ background, the additional cut $|M_Z - M_{\ell^+\ell^-}| \leq 6$ GeV has been applied.

From Figs. 11–12 is then clear that both at 10 and at 14 TeV extremely good chances of Higgs detection (for masses, say, $M_H \approx 500$ GeV) exist[12], by resorting to the two-lepton-two-neutrino channel, already for 10 inverse femtobarns. Therefore, different

[11] In fact, for $E_T^{miss} < 150$ GeV such process dominates over the others, as the jets either can escape the detector acceptance region or can be mis-measured in the calorimeter (see [4]).

[12] We have also checked that our conclusions about heavy Higgs detection are essentially unmodified if one varies the value of M_H in the region 400–700 GeV, although for higher values of the Higgs mass things are complicated by the fact that the background has a similar shape, whereas for lower

values of $\sqrt{s}_{pp}$ do not modify the search strategies of the Higgs boson via this channel and have a negligible impacts on the significances in the signal vs. background analysis.

The $H \to \ell^+\ell^-\nu_{\ell'}\bar{\nu}_{\ell'}$ channel has been claimed to give good chances for Higgs detection also for higher values of M_H, in the range 700 GeV–1 TeV. However, as in this mass region the Higgs production cross sections via the vector-vector fusion mechanism (which are comparable to the ones obtained via gluon-gluon fusion, see Figs. 5a–b in Ref. [1]) are strongly affected by unitarisation corrections to the longitudinal V_LV_L scattering (where $V = W, Z$) [36], we feel our approach (via tree–level perturbative amplitudes) inadequate to treat conveniently such delicate region of the Standard Model. This is why we preferred to restrict our attention to lower values of M_H.

4 Summary and conclusions

This paper has been devoted to study the phenomenology of the Higgs boson of the Standard Model at the Large Hadron Collider, the next generation pp collider at CERN, by comparing signal-to-background rates and by computing the corresponding significance factors. We have used in our analysis one of the most recent parton distributions as well as the most updated values of the input parameters of the $\mathcal{SM}$. We have continued here the work begun in Ref. [1], where up-to-date Higgs cross sections, branching ratios and event rates were presented.

The signatures by which Higgs detection is most promising at the LHC are the following:

- $t\bar{t}H + WH \to \ell\nu_\ell\gamma\gamma X$, in the intermediate mass range;
- $WH \to \ell\nu_\ell b\bar{b}X$ and $t\bar{t}H \to b\bar{b}b\bar{b}\ell\nu_\ell X$, in the intermediate mass range;
- $H \to Z^{(*)}Z^{(*)} \to \ell^+\ell^-\ell'^+\ell'^-$, where $\ell = e$ or μ, both in the intermediate and heavy mass range;
- $H \to ZZ \to \ell^+\ell^-\nu_{\ell'}\bar{\nu}_{\ell'}$, where $\ell = e$ or μ and $\ell' = e, \mu$ or τ, in the heavy mass range.

values the peak at soft $p_T^{\ell\ell}$ of the background largely covers the Jacobian peaks of the Higgs boson. A different optimisation of the cuts could however extend the mass range of observability of the Higgs boson via the channel $H \to \ell^+\ell^-\nu_{\ell'}\bar{\nu}_{\ell'}$.

In order to make a signal-to-background analysis as meaningful as possible, we have *consistently* evaluated both signal and background rates at leading order. This has been done because the most part of the backgrounds have been so far calculated (and here independently re-computed)[13] at lowest order only. Results have been given for the two planned CM energies of 10 and 14 TeV, and discussed on the basis of the expected integrated luminosity, 10 and/or 100 inverse femtobarns *per annum*.

What has been assessed here is the substantial complementarity of the decay channels $\gamma\gamma$ and $b\bar{b}$ in the intermediate mass range, as already noticed in Ref. [18]. In fact, the latter is the most promising in covering the mass region 80 GeV $\lesssim M_H \lesssim$ 100 GeV, whereas the former is better if 100 GeV $\lesssim M_H \lesssim$ 130 GeV. Furthermore, the option of high luminosity would make the detection much more feasible for the Higgs in the di-photon channel whereas it would reduce the chances via the $b\bar{b}$-channel, as in this case both the lepton trigger threshold and the jet p_T threshold would certainly have to be raised in order to compensate the increased trigger rates (see discussion in Ref. [18]), thus reducing even more the already low rates of both the WH and $t\bar{t}H$ signals. Finally, a sort of complementarity exists also among the latter two production mechanisms. In fact, on the one hand, the $t\bar{t}H$ signal has a quite small irreducible background in $t\bar{t}Z$ events, whereas this is not the case for WZ events, which have rates competitive with the ones of the WH signal, if $M_H \approx M_Z$. On the other hand, since the $t\bar{t}H \to \ell\nu b\bar{b}(b\bar{b})X$ signal is affected by combinatorial background, whereas $WH \to \ell\nu b\bar{b}X$ is not, the identification of Higgs signals for $M_H \not\approx M_Z$ is easier in the second case. All of this is valid for both the energy stages of the LHC, 10 and 14 TeV. In the case of poor detector performances, things would be instead quite complicated. Finally, as in general (for these two channels) the difference between the signal significances at 14 and 10 TeV is a factor of approximately 1.3–1.5, it should be considered that one should run the machine at 10 TeV twice the time that is needed at 14 TeV to get to the same threshold of observability of an intermediate mass Higgs. These conclusions, however, largely rely on the fact that the high luminosity option could be achieved in reasonable time for the $\gamma\gamma$-channel and that the expected performances of the LHC detectors (especially in photon angular and energy resolution for the $\gamma\gamma$ case and in b-tagging for the $b\bar{b}$ one) could be confirmed in practice.

[13]It made exception in this context only the usage of next-to-leading order parton distributions and of α_s at two-loops.

For 130 GeV $\lesssim M_H \lesssim 2M_Z$, the below threshold decay channel $H \to ZZ^*$ gives good chances of Higgs detection. For reasonable mass resolutions of the detectors (see Refs. [4] and [5]), and if the high luminosity option can be achieved, it should be possible an early observation of the Higgs boson, for both values of the collider energy, 10 and 14 TeV. As the peak in the ZZ^* branching ratio (i.e., below the threshold for two real Z's) occurs for $M_H = 150$ GeV, the best chances of disentangling the signals would occur for Higgs masses around this value, particularly for 10 fb^{-1} of luminosity. For such a value of $\mathcal{L}$ the case $M_H = 170$ GeV would present serious problems, independently of the mass resolution, whereas for $M_H = 130$ GeV this happens if $\Delta M \gtrsim 2$ GeV, especially at 10 TeV. The case of four muons reflects more o less the same characteristics of the total 4ℓ case.

For a heavy Higgs, with $M_H \gtrsim 2M_Z$, detection should be guaranteed up to values of ≈ 700 GeV, via the four-lepton channel. For Higgs heavier than, say, 500 GeV, the channel $H \to \ell^+\ell^-\nu_{\ell'}\bar{\nu}_{\ell'}$ will give additional/alternative possibilities. The only difficult conditions would be in the case of a very heavy Higgs boson (around 700 GeV), since in this case the corresponding decay width is very large (of the same order as the mass) and the particle cannot be considered a resonance any longer, such that the shape of the distribution in the invariant mass of the four leptons is the same as the one from the background processes. This would especially be the case at $\sqrt{s_{pp}} = 10$ TeV. In such conditions, the recourse to the channel $H \to \ell^+\ell^-\nu_{\ell'}\bar{\nu}_{\ell'}$ could turn out to be very useful, as, on the one hand, the corresponding branching ratio is six times larger than that into four leptons (so event rates would be much larger, thus allowing for larger significances) whereas, on the other hand, the signal does not suffer so strongly from broadening effects, since this latter is not a Breit-Wigner peak but a Jacobian one due to the kinematics of the Higgs.

According to the results of our analysis, we conclude that, at the latest after a few years of running at 14 TeV (the long running compensating the possible reduced performances of the detectors), the LHC might be able to *definitely* asses the correctness of the Minimal Standard Model, or to rule out this with certainty. Moreover, if the expected efficiency of the detectors will be achieved in time, then it might be possible to say something decisive about the Standard Model already after the first energy stage, around 2005.

Before closing, we would like to remind the reader two decisive aspects of the analysis that we have been carrying out, which indicate how the results we have obtained should be taken as an *indication* of the Higgs discovery potential of the LHC at its two planned stages of energy and in dependence of the integrated luminosity, more than as a complete analysis of signals, backgrounds and search strategies.

First, the analysis has been done *exclusively* but *consistently* at *parton* level. Apart from the (standard) integration procedure of the differential cross sections, no recourse to any Monte Carlo technique and/or event generator has been done. Only exact *perturbative* matrix element computations have been performed. Hadronization and fragmentation effects, jet clustering procedures, initial and final QCD and QED radiation have not been contemplated, and no special effort has been done in simulating the realistic detector performances (smearing and pile-up effects, finite efficiency in lepton identification, conversion losses for photons, etc ...), other than adopting the usual selection criteria, which can be largely implemented also at parton level (transverse momenta and (pseudo)rapidity of leptons and jets, angular separations, missing energy, etc ...). Therefore, a systematic uncertainty due to the unavoidable differences between parton-level and jet-level procedures come with our results. The interplay between these two approaches has been carefully investigated and quantified in Ref. [18], in the case of the $b\bar{b}$ channel. In general, the differences are larger for processes with a complex and various final state topology (such as the one involving top production and decay), and they mainly concern the treatment of hadronic final states, more than the one of leptons and neutrinos. This observation can be safely extended to involve also the case of the other Higgs decay channels (and relative backgrounds). However, we do not expect the inclusion of all these non-perturbative aspects to wash out the main results that have been assessed here, also because many of the Higgs signatures studied in this paper were indeed non-hadronic (i.e., $H \to \gamma\gamma, 4\ell, 2l2\nu$). In contrast, many of the inconsistencies that often occur in such kind of analyses (for example, when NLO order computations are compared to LO results, when out-of-date parton distributions are used, when parton shower approximations are substituted to or interfaced with exact computations, etc ...) are here totally removed.

Second, it has to be remembered that higher order rates for the most part of the backgrounds have not been computed yet. Therefore, especially when proceeding to a signal-to-background analysis at lowest order (thus avoiding the use of K-factors for the signals, as it has been done here), an overall uncertainty due to the lack of knowledge of next-to-leading order corrections remains. This has been estimated, for example, for the case of the WH signal and corresponding backgrounds, in Ref. [37], where it was shown that their inclusion does not change the final results significantly. Once all the rates needed for a self-consistent signal-to-background analysis will be available at next-to-leading order, very accurate predictions about the prospects of Higgs detection and study at the LHC will be given[14]. It is hard to think, in fact, that next-to-next-to-leading corrections can significantly modify the conclusions obtained at the preceeding order. Possibly, an important exception could be the case of the gluon-gluon fusion process, $gg \rightarrow H$, for which these could well be large, as the next-to-leading rates differ by $\approx$ 100% from the leading order ones [1]. Because of the crucial role that this production channel has at the LHC, it is important that such corrections are soon investigated.

Finally, we remind the reader that the top mass is no longer a significant source of theoretical error in Higgs searches, as this particle has been finally identified at FNAL and its mass measured rather accurately, i.e., $m_t = 175 \pm 6$ GeV. Certainly, there is a residual uncertainty in the predictions involving the production of (virtual or real) t-quarks due to the existing experimental error. However it has been shown (see Fig. 6 in Ref. [1]) that its impact on the Higgs production rates is generally small, yielding differences in the cross sections which are generally below $8 - 9\%$. We have verified that similar effects also occur in the case of the top backgrounds. The only exceptions are the NLO rates for the signal $gg \rightarrow H$ (via top loops), for which such differences can be as large as 30% (near the threshold $M_H \approx 2m_t$). However, this has a limited phenomenological relevance, as for that value of M_H the Higgs signals are well above the backgrounds (see, e.g., Fig. 9a and 10a and compare to the rates given in the two tables of Ref. [1]). Furthermore, one should remember that by the time the LHC comes into operation the top quark mass will be known with much better precision so that the accuracy in the prediction of top cross sections will be even higher than that discussed in this paper.

[14]In this respect, we inform the reader that the calculation of the complete QCD corrections at NLO to the $pp \rightarrow t\bar{t}H$ production channel are now well under way [38].

5 Acknowledgments

This work is supported in part by the Ministero dell' Università e della Ricerca Scientifica, by the UK Particle Physics and Astronomy Research Council and by the EC Programme "Human Capital and Mobility", contract CHRX–CT–93–0357 (DG 12 COMA). We are grateful to E. Maina for a careful reading of the manuscript and to W.J. Stirling for useful suggestions. We would also like to thank all the members of the Centre for Particle Theory of Durham University (and among them, in particular, Mike Whalley, for his incomparable help in 'digging' me out of tricky computing problems), where the most part of this work has been carried out, for hosting me during eighteen friendly and scientifically stimulating months.

References

[1] Z. Kunszt, S. Moretti and W.J. Stirling, *preprint* DFTT 34/95, DTP/96/100, Cavendish-HEP-96/20, ETH-TH-96/48, November 1996.

[2] See, for example:
Review of Particle Properties, *Phys. Rev.* **D45** (1992) S1.

[3] Proceedings of the "*Large Hadron Collider Workshop*", Aachen, 4–9 October 1990, eds. G. Jarlskog and D. Rein, Report CERN 90–10, ECFA 90–133, Geneva, 1990.

[4] ATLAS Technical Proposal, CERN/LHC/94-43 LHCC/P2 (December 1994).

[5] CMS Technical Proposal, CERN/LHC/94-43 LHCC/P1 (December 1994).

[6] T. Sjöstrand, "High-Energy-Physics Event Generation with PYTHIA 5.7 and jetSET 7.4", CERN *preprints* CERN-TH.7111/93 and CERN-TH.7112/93;
G. Marchesini, B.R. Webber *et al.*, *Comput. Phys. Commun.* **67** (1992) 465;
GEANT, Detector Description and Simulation Tool, CERN Program Library Q123.

[7] T. Stelzer and W.F. Long, *Comp. Phys. Comm.* **81** (1994) 357.

[8] E. Murayama, I. Watanabe and K. Hagiwara, HELAS: HELicity Amplitude Subroutines for Feynman Diagram Evaluations, *KEK Report* 91-11, January 1992.

[9] G.P. Lepage, *Jour. Comp. Phys.* **27** (1978) 192.

[10] A.D. Martin, R.G. Roberts and W.J. Stirling, *Phys. Rev.* **D50** (1994) 6734.

[11] CDF Collaboration, *Phys. Rev. Lett.* **74** (1995) 2626.

[12] D0 Collaboration, *Phys. Rev. Lett.* **74** (1995) 2632.

[13] A. Caner, Presented at "*Rencontres du Physique de la Valle d'Aoste*", March 1996;
M. Narain, Presented at the '*Rencontres du Physique de la Valle d'Aoste*", March 1996;
P. Grannis, talk presented at ICHEP96, Warsaw, Poland, 25-31 July 1996, to appear in the proceedings.

[14] J.H. Kühn, *Act. Phys. Pol.* **B12** (1981) 347;
J.H. Kühn, *Act. Phys. Austr. Suppl.* **XXIV** (1982) 203.

[15] J.P. Martin, talk presented at ICHEP96, Warsaw, Poland, 25-31 July 1996, to appear in the proceedings.

[16] See, for example:
A. Blondel, plenary talk presented at ICHEP96, Warsaw, Poland, 25-31 July 1996, to appear in the proceedings.

[17] M. Dittmar and H. Dreiner, *preprint* RAL-96-049 August 1996.

[18] D. Froidevaux and E. Richter-Was, *Z. Phys.* **C67** (1995) 213.

[19] L. Fayard and G. Unal, EAGLE Internal Note PHYS-NO-001 and Addenda 1 & 2.

[20] C. Seez *et al.*, in Ref. [3].

[21] A. Ballestrero and E. Maina, *Phys. Lett.* **B268** (1992) 437.

[22] E. Maina and S. Moretti, *Phys. Lett.* **B286** (1992) 370.

[23] V. Barger, T. Han, J. Ohnemus and D. Zeppenfeld, *Phys. Rev. Lett.* **62** (1989) 1971; *Phys. Rev.* **D40** (1989) 2888; *ibidem* **D41** (1990) 1715 (Erratum).

[24] J. Dai, J.F. Gunion and R. Vega, *Phys. Rev. Lett.* **71** (1993) 2699.

[25] *Solenoidal Detector Collaboration Technical Design Report*, E.L. Berger *et al.*, *Report* SDC–92–201, SSCL–SR–12

[26] A. Stange, W. Marciano and S.S.D. Willenbrock, *Phys. Rev.* **D49** (1994) 1354; *ibidem* **D50** (1994) 4491.

[27] J.F. Gunion and T. Han, *Phys. Rev.* **D51** (1995) 1051.

[28] S.L. Glashow, D.V. Nanopoulos and A. Yildiz, *Phys. Rev.* **D18** (1978) 1724.

[29] M. Della Negra *et al.*, in Ref. [3].

[30] M. Dzelalija and R. Kinnunen, CMS *internal note* CMS TN/94-214 (1994).

[31] U. Baur and E.W.N. Glover, *Nucl. Phys.* **B347** (1990) 12;
U. Baur and E.W.N. Glover, in Ref. [3].

[32] R. Kleiss and J.J. van der Bij, in Ref. [3].

[33] E.W.N. Glover and J.J. van der Bij, *Nucl. Phys.* **B321** (1989) 561.

[34] N. Stepanov and A. Starodumov, CMS *internal note* CMS TN/92-49 (1992);
N. Stepanov, CMS *internal note* CMS TN/93-87 (1993).

[35] I. Zuckerman *et al.*, ATLAS *internal note* PHYS-NO-007 (1992);
M. Bosman and M. Nessi, ATLAS *internal note* PHYS-NO-050 (1994).

[36] A. Hasenfratz, K. Jansen, C. Lang, T. Neuhaus and H. Yoneyama, *Phys. Lett.* **B199** (1987) 531;
J. Kuti, L. Liu and Y. Shen, *Phys. Rev. Lett.* **61** (1988) 678;
M. Lüscher and P. Weisz, *Nucl. Phys.* **B318** (1989) 705.

[37] T. Han and S.S.D. Willenbrock, *Phys. Lett.* **B273** (1991) 167.

[38] B.K. Bullock and S. Moretti, in preparation.

Table captions

[I] Number of signal (S, $WH + t\bar{t}H$) and background (B, $W\gamma\gamma + W\gamma j + t\bar{t}\gamma\gamma + t\bar{t}\gamma + Z\gamma$) events, together with the significance $S/\sqrt{B}$, for the signature $\ell\gamma\gamma X$, in the windows $|M_H - M_{\gamma\gamma}| < 1(2)[3]$ GeV, for $\mathcal{L} = 100$ fb^{-1} and the selection of Higgs masses $M_H = 80, 100$ and 120 GeV, after the cuts mentioned in the text, at $\sqrt{s_{pp}} = 10$ TeV (upper section) and 14 TeV (lower section), for $m_t = 175$ GeV. In order to suppress the background $Z\gamma$ the additional cut $|M_Z - M_{\ell\gamma}| > 5$ GeV is applied.

[II] Number of signal (S, WH) and background (B, $WZ + Wb\bar{b} + t\bar{b} + t\bar{t} + t\bar{b}q + Wjj + Wbj$) events, together with the significance $S/\sqrt{B}$, for the signature $\ell b\bar{b}X$, in the window $|M_H - M_{b\bar{b}}| < 15$ GeV, for $\mathcal{L} = 10$ fb^{-1} and the selection of Higgs masses $M_H = 80, 100$ and 120 GeV, after the cuts mentioned in the text, at $\sqrt{s_{pp}} = 10$ TeV (upper section) and 14 TeV (lower section), for $m_t = 175$ GeV. The b-tagging performances are $\epsilon_b = 50\%$ and $R = 50$.

[III] Number of signal (S, $t\bar{t}H$) and background (B, $t\bar{t}Z + t\bar{t}j + Wjjj + t\bar{t} + t\bar{b}q$) events, together with the significance $S/\sqrt{B}$, for the signature $\ell b\bar{b}bX$, in the window $|M_H - M_{b\bar{b}}| < 15$ GeV, for $\mathcal{L} = 10$ fb^{-1} and the selection of Higgs masses $M_H = 80, 100$ and 120 GeV, after the cuts mentioned in the text, at $\sqrt{s_{pp}} = 10$ TeV (upper section) and 14 TeV (lower section), for $m_t = 175$ GeV. The b-tagging performances are $\epsilon_b = 50\%$ and $R = 50$ (lower row), $\epsilon_b = 70\%$ and $R = 10$ (upper row).

[IV] Number of signal (S, $H + q\bar{q}H$) and background (B, $t\bar{t} + Zb\bar{b} + ZZ^*$) events, together with the significance $S/\sqrt{B}$, for the signature $4\ell X$, in the windows $|M_H - M_{4\ell}| < 1(2)[3]$ GeV, for $\mathcal{L} = 100$ fb^{-1} and the selection of Higgs masses $M_H = 130, 150$ and 170 GeV, after the cuts mentioned in the text, at $\sqrt{s_{pp}} = 10$ TeV (upper section) and 14 TeV (lower section), for $m_t = 175$ GeV. In order to suppress the background $t\bar{t}$ the additional cut $|M_Z - M_{\ell^+\ell^-}| < 10$ GeV is applied.

[V] Number of signal (S, $H + q\bar{q}H$) and background (B, $t\bar{t} + Zb\bar{b} + ZZ^*$) events, together with the significance $S/\sqrt{B}$, for the signature $4\mu X$, in the windows $|M_H - M_{4\mu}| < 1(2)[3]$ GeV, for $\mathcal{L} = 100$ fb^{-1} and the selection of Higgs masses

$M_H = 130, 150$ and 170 GeV, after the cuts mentioned in the text, at $\sqrt{s}_{pp} = 10$ TeV (upper section) and 14 TeV (lower section), for $m_t = 175$ GeV. In order to suppress the background $t\bar{t}$ the additional cut $|M_Z - M_{\mu^+\mu^-}| < 10$ GeV is applied.

Figure captions

[1] Distribution in invariant mass of the photon-photon pair for signal ($WH + t\bar{t}H$) and background ($W\gamma\gamma + W\gamma j + t\bar{t}\gamma\gamma + t\bar{t}\gamma + Z\gamma$), giving the signature $\ell\gamma\gamma X$, after the cuts mentioned in the text, at $\sqrt{s}_{pp} = 10$ TeV and for $m_t = 175$ GeV (a). In order to suppress the background $Z\gamma$ the additional cut $|M_Z - M_{\ell\gamma}| > 5$ GeV is applied. The symbol ε indicates that also the reduction factors due to misidentification of a lepton or a jet for a photon are included, in the case of the backgrounds $Z\gamma$, $t\bar{t}\gamma$ and $W\gamma j$. In (b) the various background contributions are shown separately (with $m_t = 175$ GeV for top contributions).

[2] Same as Fig. 1, for $\sqrt{s}_{pp} = 14$ TeV.

[3] Distribution in invariant mass of the $b\bar{b}$–pair for signal (WH) and background ($WZ + Wb\bar{b} + t\bar{b} + t\bar{t} + t\bar{b}q + Wbj + Wjj$), giving the signature $\ell b\bar{b}X$, after the cuts mentioned in the text, at $\sqrt{s}_{pp} = 10$ TeV and for $m_t = 175$ GeV (a). In the case of the backgrounds $t\bar{t}$ and $t\bar{b}q$ we have also implemented the cuts indicated in the text for the additional jets in the final state. The symbol ε indicates that efficiencies and reduction factors of b-tagging are included, both for signals and backgrounds. In (b) the various background contributions are shown separately (with $m_t = 175$ GeV for top contributions).

[4] Same as Fig. 3, for $\sqrt{s}_{pp} = 14$ TeV.

[5] Distribution in invariant mass of the two lepton pairs for the sum of signal ($H + q\bar{q}H$) and background ($t\bar{t} + Zb\bar{b} + ZZ^*$, the latter in shadowing), giving the signature $4\ell X$, after the cuts mentioned in the text, at $\sqrt{s}_{pp} = 10$ TeV and for $m_t = 175$ GeV. In order to suppress the background $t\bar{t}$ the additional cut $|M_Z - M_{\ell^+\ell^-}| < 10$ GeV is applied.

[6] Same as Fig. 5, for $\sqrt{s}_{pp} = 14$ TeV.

[7] Distribution in invariant mass of the four muons for the sum of signal ($H + q\bar{q}H$) and background ($t\bar{t} + Zb\bar{b} + ZZ^*$, the latter in shadowing), giving the signature $4\mu X$, after the cuts mentioned in the text, at $\sqrt{s}_{pp} = 10$ TeV and for $m_t = 175$ GeV. In order to suppress the background $t\bar{t}$ the additional cut $|M_Z - M_{\mu^+\mu^-}| < 10$ GeV is applied.

[8] Same as Fig. 7, for $\sqrt{s}_{pp} = 14$ TeV.

[9] Distribution in invariant mass of the two lepton pairs for signal ($H + q\bar{q}H$, in shadowing) and background (ZZ), giving the signature $4\ell X$, after the cuts mentioned in the text, at $\sqrt{s}_{pp} = 10$ TeV, for $m_t = 175$ GeV and for $M_H = 300$ (a), 500 (b) and 700 (c) GeV.

[10] Same as Fig. 9, for $\sqrt{s}_{pp} = 14$ TeV.

[11] Distribution in transverse momentum of the lepton pair for signal ($H + q\bar{q}H$, in shadowing) and background ($ZZ + ZW + t\bar{t} + \; Z + \text{jets}$), giving the signature $\ell^+\ell^-\nu_{\ell'}\bar{\nu}_{\ell'}X$, after the cuts mentioned in the text, at $\sqrt{s}_{pp} = 10$ TeV, for $m_t = 175$ GeV and for $M_H = 500$ GeV. In order to suppress the background $t\bar{t}$ the additional cut $|M_Z - M_{\ell^+\ell^-}| \leq 6$ GeV is applied.

[12] Same as Fig. 11, for $\sqrt{s}_{pp} = 14$ TeV.

$\ell\gamma\gamma X$			
M_H (GeV)	S	B/2 GeV	$S/\sqrt{B}$
80	28.6	6.9	10.9(7.7)[6.3]
100	37.7	5.5	16.1(11.4)[9.3]
120	37.9	4.0	18.9(13.4)[10.9]
$\sqrt{s}_{pp} = 10$ TeV			
80	44.6	9.7	14.3(10.1)[8.3]
100	59.0	8.0	20.9(14.8)[12.0]
120	60.0	6.1	24.3(17.2)[14.0]
$\sqrt{s}_{pp} = 14$ TeV			
$m_t = 175$ GeV			

Tab. I

$\ell b\bar{b}X$ (Events/30 GeV)			
80	224	460	10.
100	140	323	7.8
120	74	255	4.6
$\sqrt{s}_{pp} = 10$ TeV			
80	299	715	11.
100	187	517	8.2
120	100	411	4.9
$\sqrt{s}_{pp} = 10$ TeV			
$m_t = 175$ GeV			

Tab. II

$\ell b\bar{b}bX$ (Events/30 GeV)			
M_H (GeV)	S	B	$S/\sqrt{B}$
80	46	177	3.6
	17	27	3.3
100	27	176	2.0
	10	26	2.0
120	14	165	1.1
	5	23	1.0
$\sqrt{s}_{pp} = 10$ TeV			
80	98	335	5.4
	35	54	4.8
100	57	341	3.1
	21	51	2.9
120	30	318	1.7
	11	46	1.6
$\sqrt{s}_{pp} = 14$ TeV			
$m_t = 175$ GeV			

Tab. III

$4\ell X$			
M_H (GeV)	S	$B/2$ GeV	$S/\sqrt{B}$
130	44.7	19.0	10.3(7.4)[6.1]
150	103.6	11.82	30.1(21.0)[17.1]
170	20.6	6.8	7.9(5.7)[4.7]
$\sqrt{s}_{pp} = 10$ TeV			
130	74.3	26.0	14.6(10.2)[8.3]
150	151.1	15.6	38.3(27.1)[22.1]
170	34.2	12.4	9.7(6.7)[5.5]
$\sqrt{s}_{pp} = 14$ TeV			
$m_t = 175$ GeV			

Tab. IV

$4\mu X$			
M_H (GeV)	S	$B/2$ GeV	$S/\sqrt{B}$
130	28.3	13.5	7.7(5.3)[4.3]
150	55.6	8.2	19.4(13.7)[11.2]
170	10.4	4.3	5.0(3.6)[3.0]
$\sqrt{s}_{pp} = 10$ TeV			
130	44.9	17.3	10.8(7.5)[6.1]
150	90.9	10.1	28.6(20.2)[16.5]
170	17.4	8.2	6.1(4.4)[3.6]
$\sqrt{s}_{pp} = 14$ TeV			
$m_t = 175$ GeV			

Tab. V

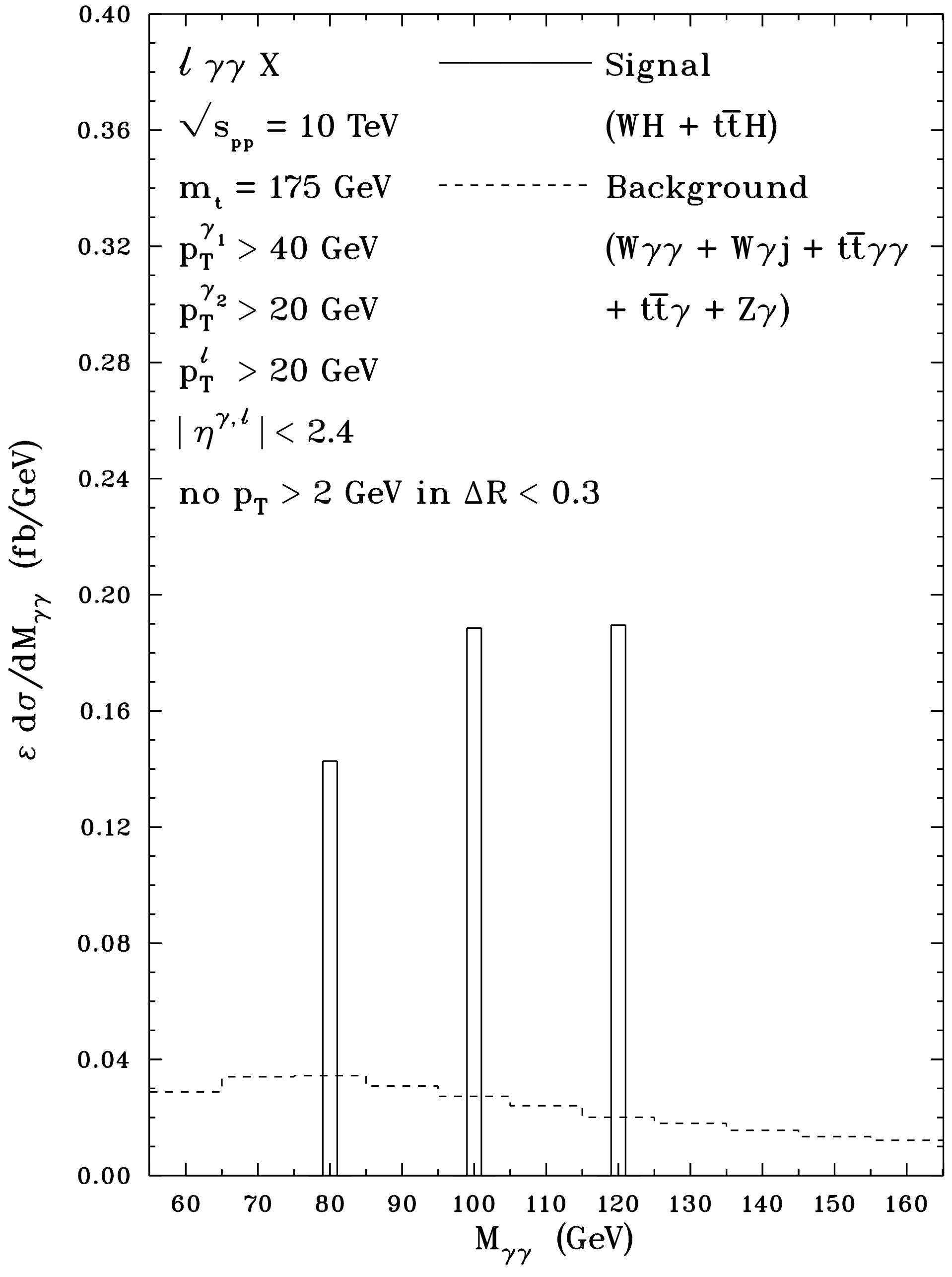
$\ell\,\gamma\gamma$ X
$\sqrt{s_{pp}}$ = 10 TeV
m_t = 175 GeV
$p_T^{\gamma_1} > 40$ GeV
$p_T^{\gamma_2} > 20$ GeV
$p_T^{\ell} > 20$ GeV
$|\eta^{\gamma,\ell}| < 2.4$
no $p_T > 2$ GeV in $\Delta R < 0.3$
Signal
(WH + $t\bar{t}$H)
Background
(W$\gamma\gamma$ + Wγj + $t\bar{t}\gamma\gamma$
+ $t\bar{t}\gamma$ + Zγ)
$\varepsilon\ d\sigma/dM_{\gamma\gamma}$ (fb/GeV)
$M_{\gamma\gamma}$ (GeV)
0.00
0.04
0.08
0.12
0.16
0.20
0.24
0.28
0.32
0.36
0.40
60
70
80
90
100
110
120
130
140
150
160

Fig. 1a

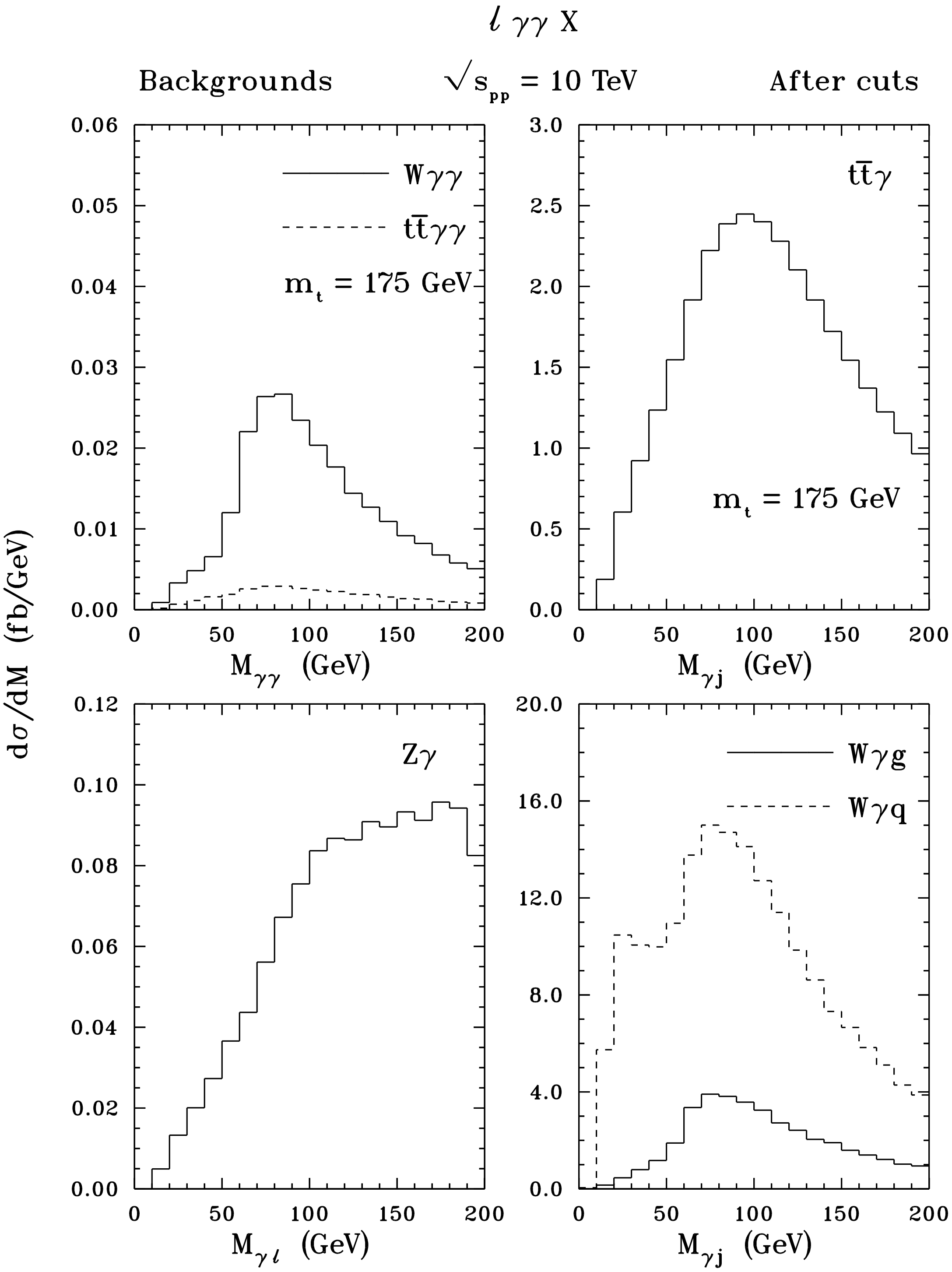

$\ell\,\gamma\gamma$ X
Backgrounds
$\sqrt{s_{pp}}$ = 10 TeV
After cuts
$d\sigma/dM$ (fb/GeV)
$W\gamma\gamma$
$t\bar{t}\gamma\gamma$
m_t = 175 GeV
$M_{\gamma\gamma}$ (GeV)
$t\bar{t}\gamma$
m_t = 175 GeV
$M_{\gamma j}$ (GeV)
$Z\gamma$
$M_{\gamma\ell}$ (GeV)
$W\gamma g$
$W\gamma q$
$M_{\gamma j}$ (GeV)

Fig. 1b

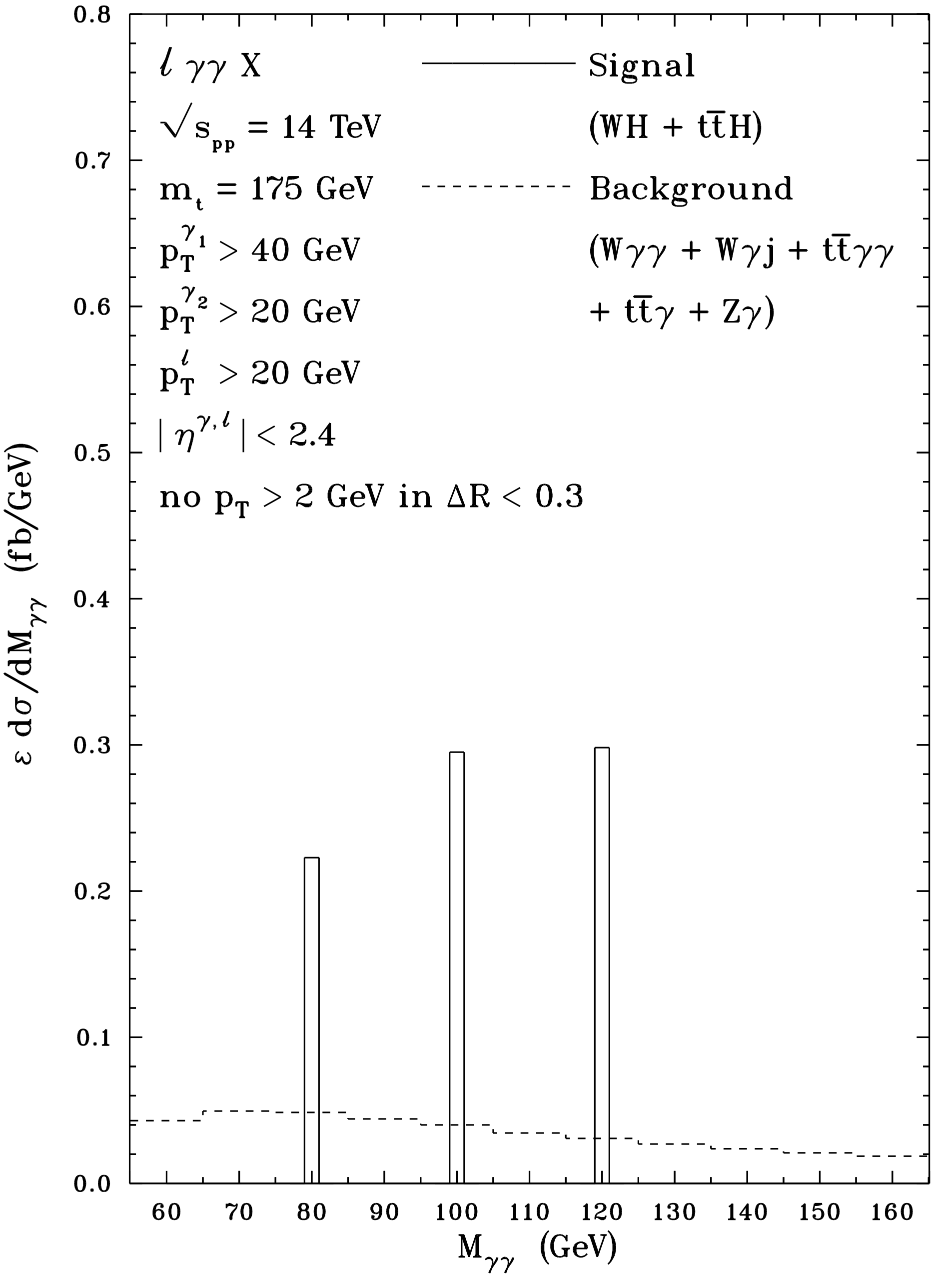

0.8
0.7
0.6
0.5
0.4
0.3
0.2
0.1
0.0
$\ell\ \gamma\gamma$ X
$\sqrt{s_{pp}}$ = 14 TeV
m_t = 175 GeV
$p_T^{\gamma_1} > 40$ GeV
$p_T^{\gamma_2} > 20$ GeV
$p_T^{\ell} > 20$ GeV
$|\eta^{\gamma,\ell}| < 2.4$
no $p_T > 2$ GeV in $\Delta R < 0.3$
Signal
(WH + $t\bar{t}$H)
Background
(W$\gamma\gamma$ + Wγj + $t\bar{t}\gamma\gamma$
+ $t\bar{t}\gamma$ + Zγ)
$\varepsilon\ d\sigma/dM_{\gamma\gamma}$ (fb/GeV)
60
70
80
90
100
110
120
130
140
150
160
$M_{\gamma\gamma}$ (GeV)

Fig. 2a

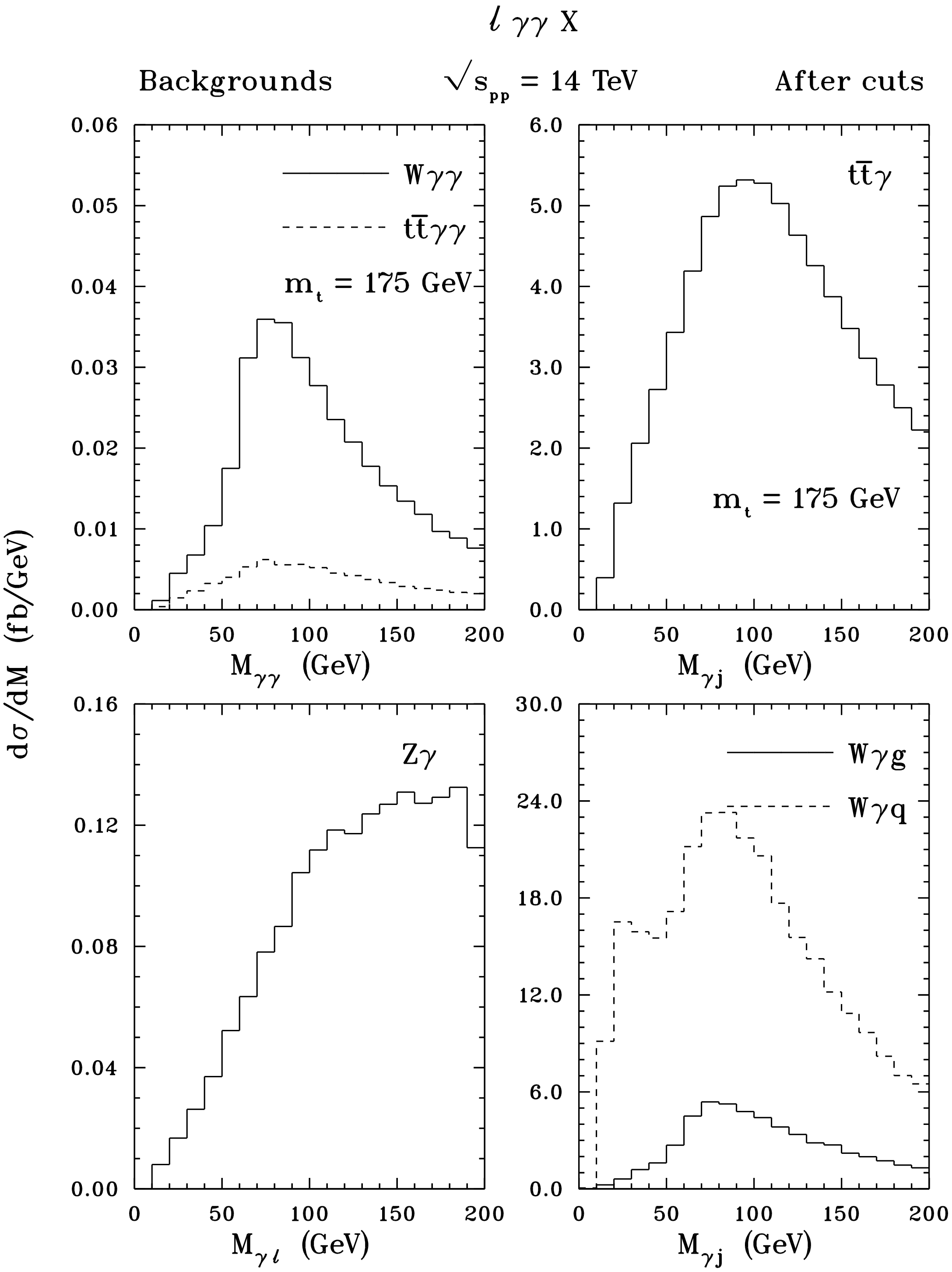

ℓ γγ X
Backgrounds
√s_pp = 14 TeV
After cuts
dσ/dM (fb/GeV)
Wγγ
tt̄γγ
m_t = 175 GeV
M_γγ (GeV)
tt̄γ
m_t = 175 GeV
M_γj (GeV)
Zγ
M_γℓ (GeV)
Wγg
Wγq
M_γj (GeV)

Fig. 2b

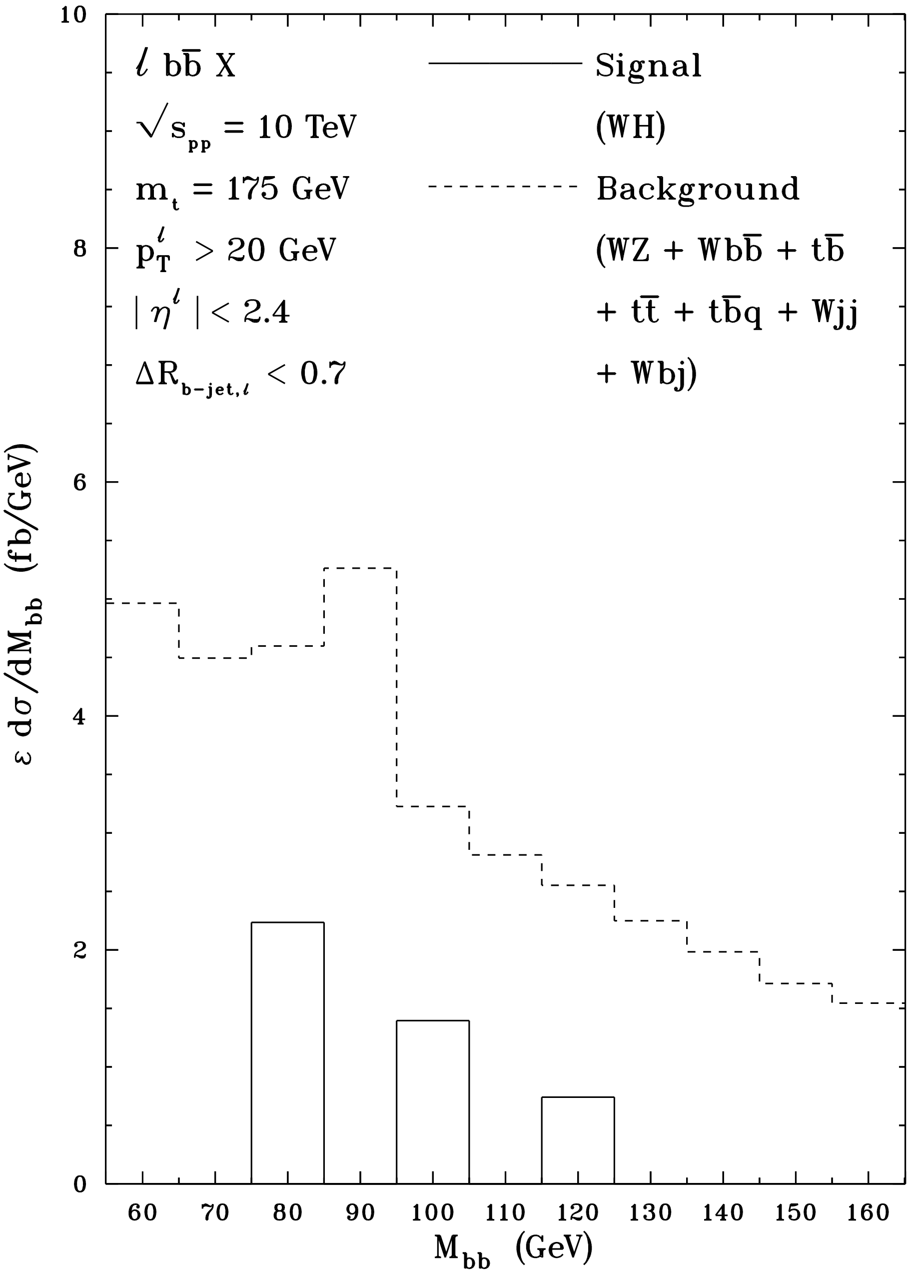
$\ell\, b\bar{b}\, X$
$\sqrt{s_{pp}}$ = 10 TeV
m_t = 175 GeV
p_T^ℓ > 20 GeV
$|\eta^\ell| < 2.4$
$\Delta R_{b\text{-jet},\ell} < 0.7$
Signal
(WH)
Background
(WZ + Wb$\bar{b}$ + t$\bar{b}$
+ t$\bar{t}$ + t$\bar{b}$q + Wjj
+ Wbj)
$\varepsilon\, d\sigma/dM_{bb}$ (fb/GeV)
M_{bb} (GeV)
0
2
4
6
8
10
60
70
80
90
100
110
120
130
140
150
160

Fig. 3a

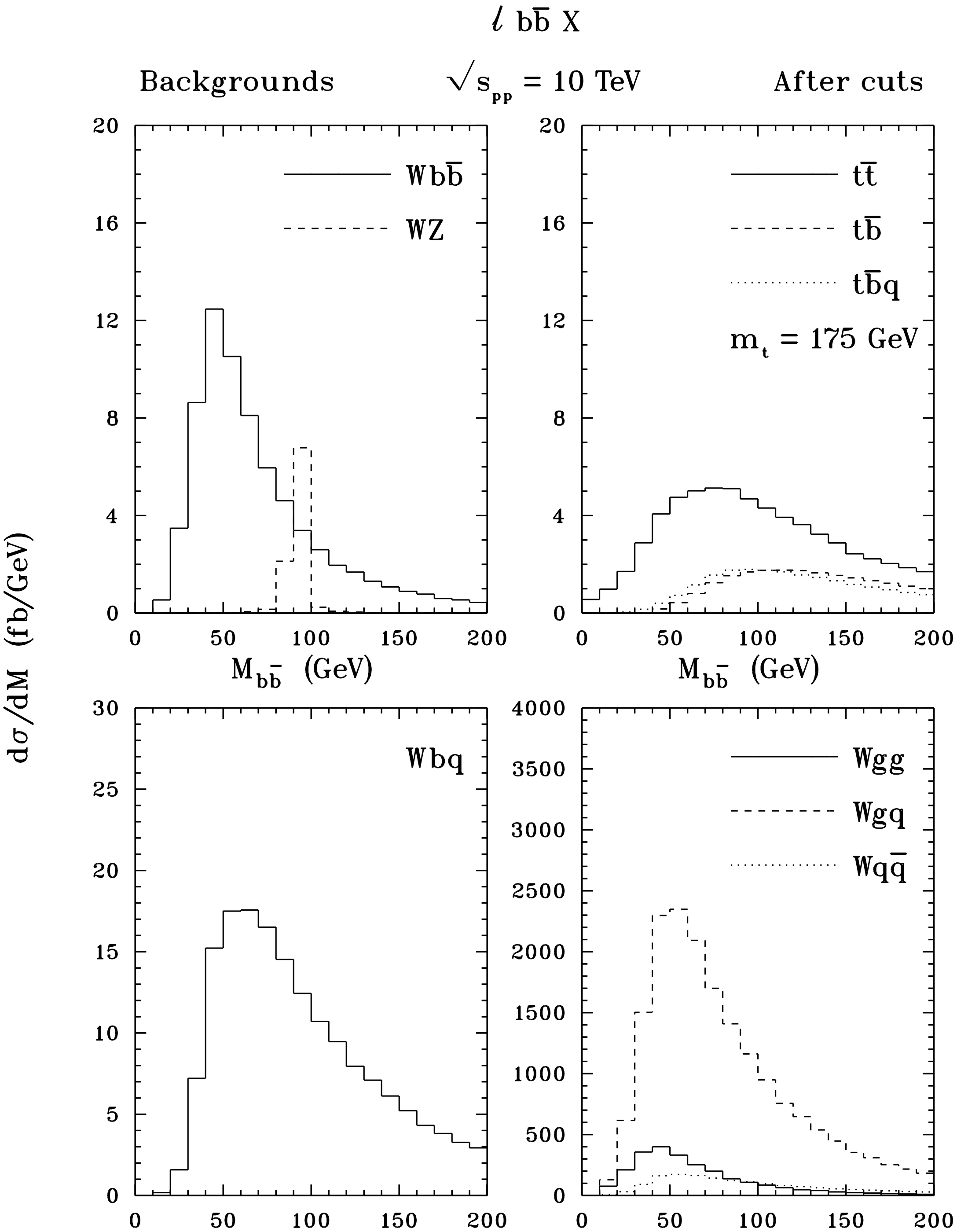
ℓ b$\bar{b}$ X
Backgrounds
$\sqrt{s_{pp}}$ = 10 TeV
After cuts
Wb$\bar{b}$
WZ
t$\bar{t}$
t$\bar{b}$
t$\bar{b}$q
m_t = 175 GeV
Wbq
Wgg
Wgq
Wq$\bar{q}$
$M_{b\bar{b}}$ (GeV)
M_{bj} (GeV)
M_{jj} (GeV)
$d\sigma/dM$ (fb/GeV)

Fig. 3b

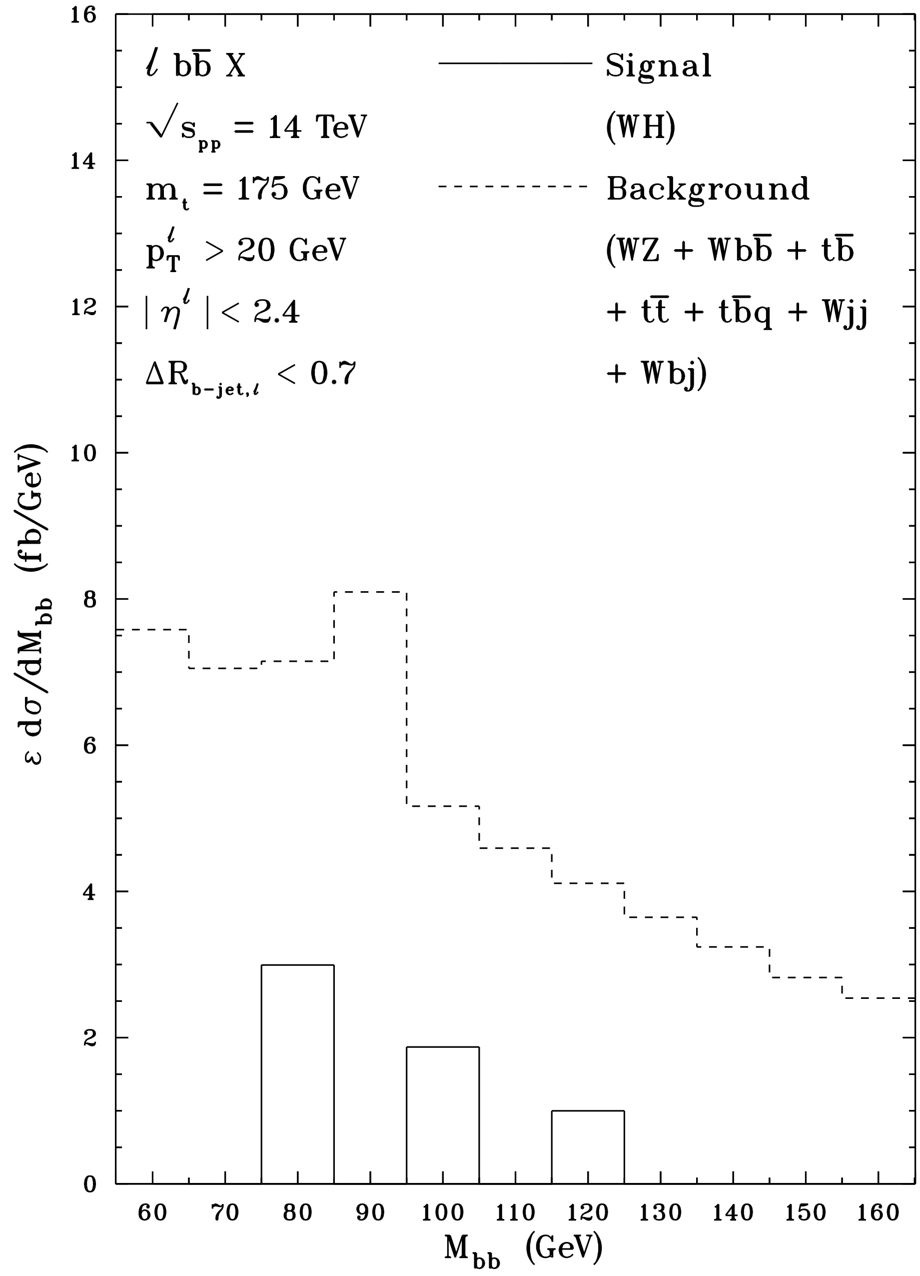

ℓ b$\bar{b}$ X
$\sqrt{s_{pp}}$ = 14 TeV
m_t = 175 GeV
p_T^ℓ > 20 GeV
$|\eta^\ell| < 2.4$
$\Delta R_{b-jet,\ell} < 0.7$
Signal
(WH)
Background
(WZ + Wb$\bar{b}$ + t$\bar{b}$
+ t$\bar{t}$ + t$\bar{b}$q + Wjj
+ Wbj)
$\varepsilon\, d\sigma/dM_{bb}$ (fb/GeV)
M_{bb} (GeV)

Fig. 4a

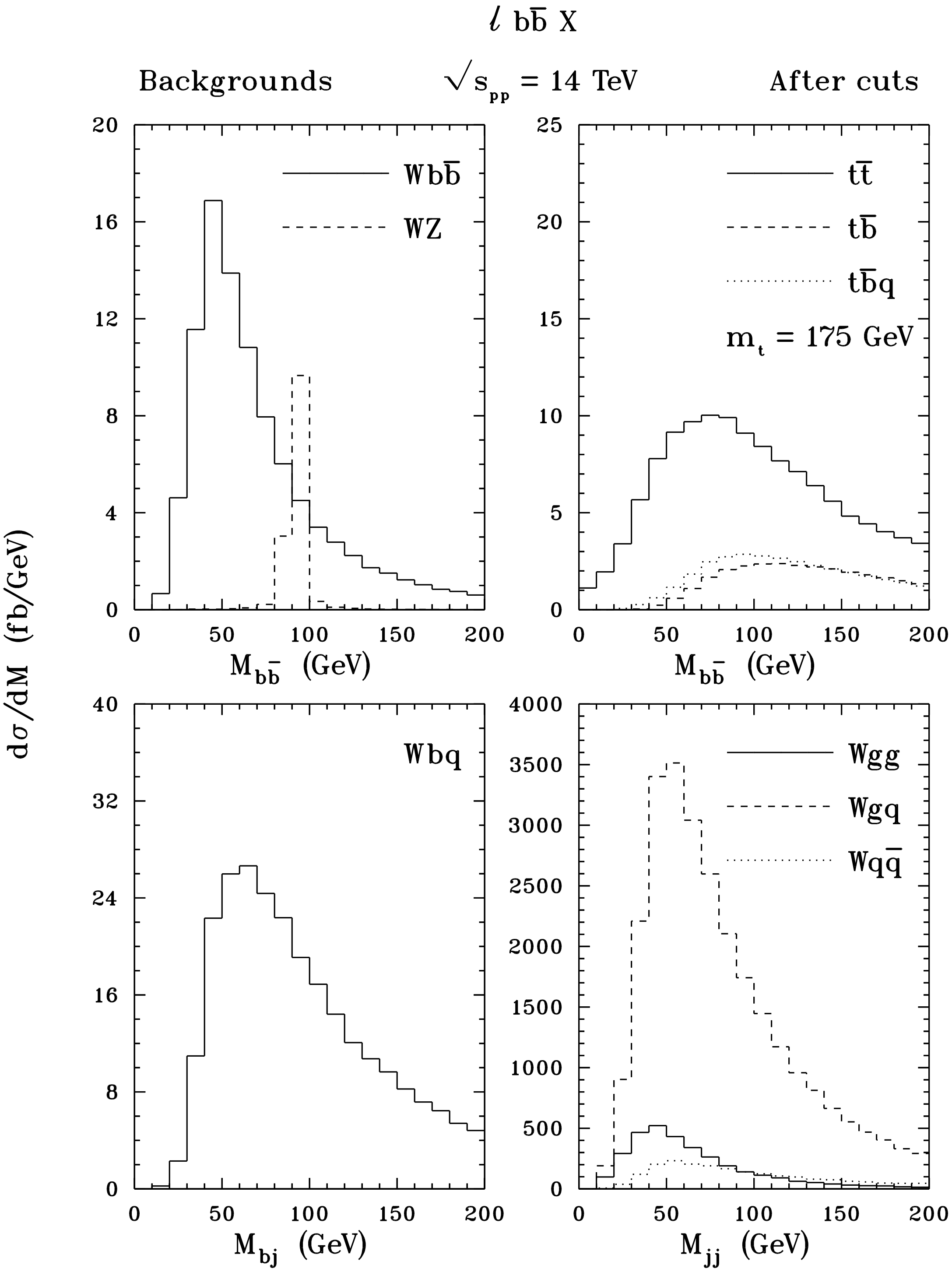

$\ell\, b\bar{b}\, X$
Backgrounds
$\sqrt{s_{pp}}$ = 14 TeV
After cuts
$d\sigma/dM$ (fb/GeV)
$Wb\bar{b}$
WZ
$M_{b\bar{b}}$ (GeV)
$t\bar{t}$
$t\bar{b}$
$t\bar{b}q$
m_t = 175 GeV
$M_{b\bar{b}}$ (GeV)
Wbq
M_{bj} (GeV)
Wgg
Wgq
$Wq\bar{q}$
M_{jj} (GeV)

Fig. 4b

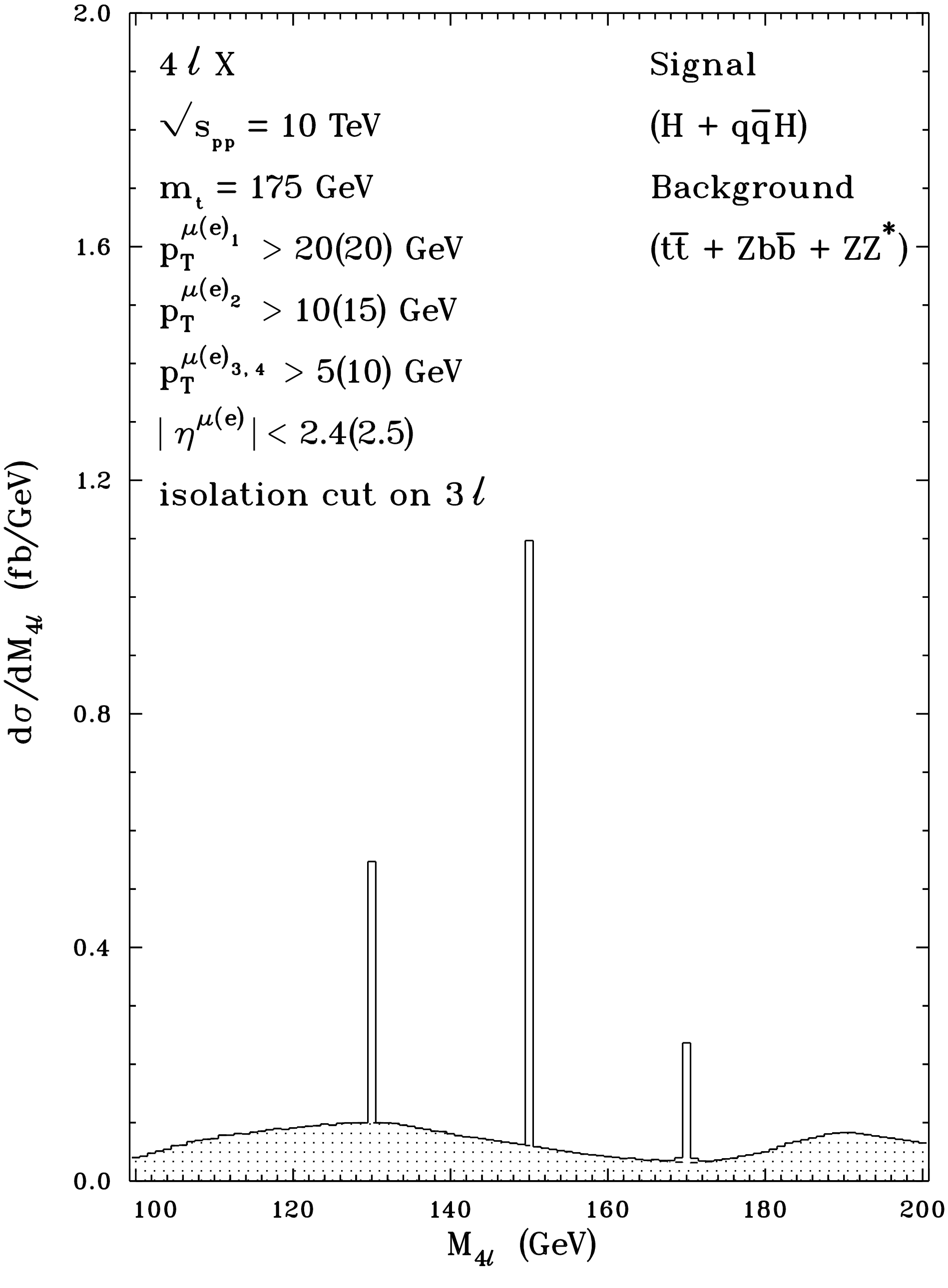

2.0
1.6
1.2
0.8
0.4
0.0
100
120
140
160
180
200
4 ℓ X
$\sqrt{s_{pp}}$ = 10 TeV
m_t = 175 GeV
$p_T^{\mu(e)_1}$ > 20(20) GeV
$p_T^{\mu(e)_2}$ > 10(15) GeV
$p_T^{\mu(e)_{3,4}}$ > 5(10) GeV
$|\eta^{\mu(e)}|$ < 2.4(2.5)
isolation cut on 3 ℓ
Signal
($H + q\bar{q}H$)
Background
($t\bar{t} + Zb\bar{b} + ZZ^*$)
$d\sigma/dM_{4\ell}$ (fb/GeV)
$M_{4\ell}$ (GeV)

Fig. 5

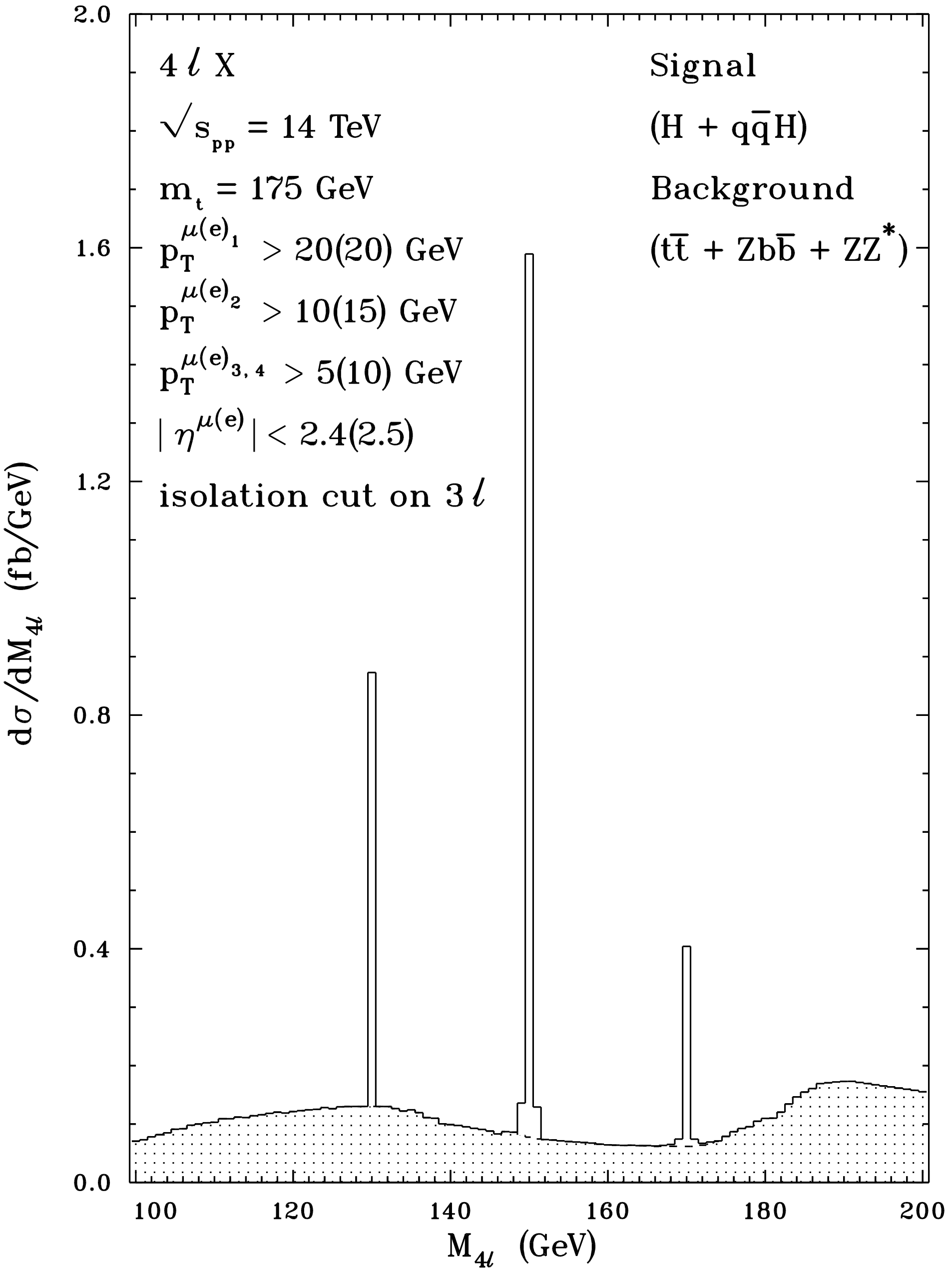
4 ℓ X
√s_pp = 14 TeV
m_t = 175 GeV
p_T^{μ(e)_1} > 20(20) GeV
p_T^{μ(e)_2} > 10(15) GeV
p_T^{μ(e)_{3,4}} > 5(10) GeV
| η^{μ(e)} | < 2.4(2.5)
isolation cut on 3 ℓ
Signal
(H + qq̄H)
Background
(tt̄ + Zbb̄ + ZZ*)
dσ/dM_4ℓ (fb/GeV)
M_4ℓ (GeV)
0.0
0.4
0.8
1.2
1.6
2.0
100
120
140
160
180
200

Fig. 6

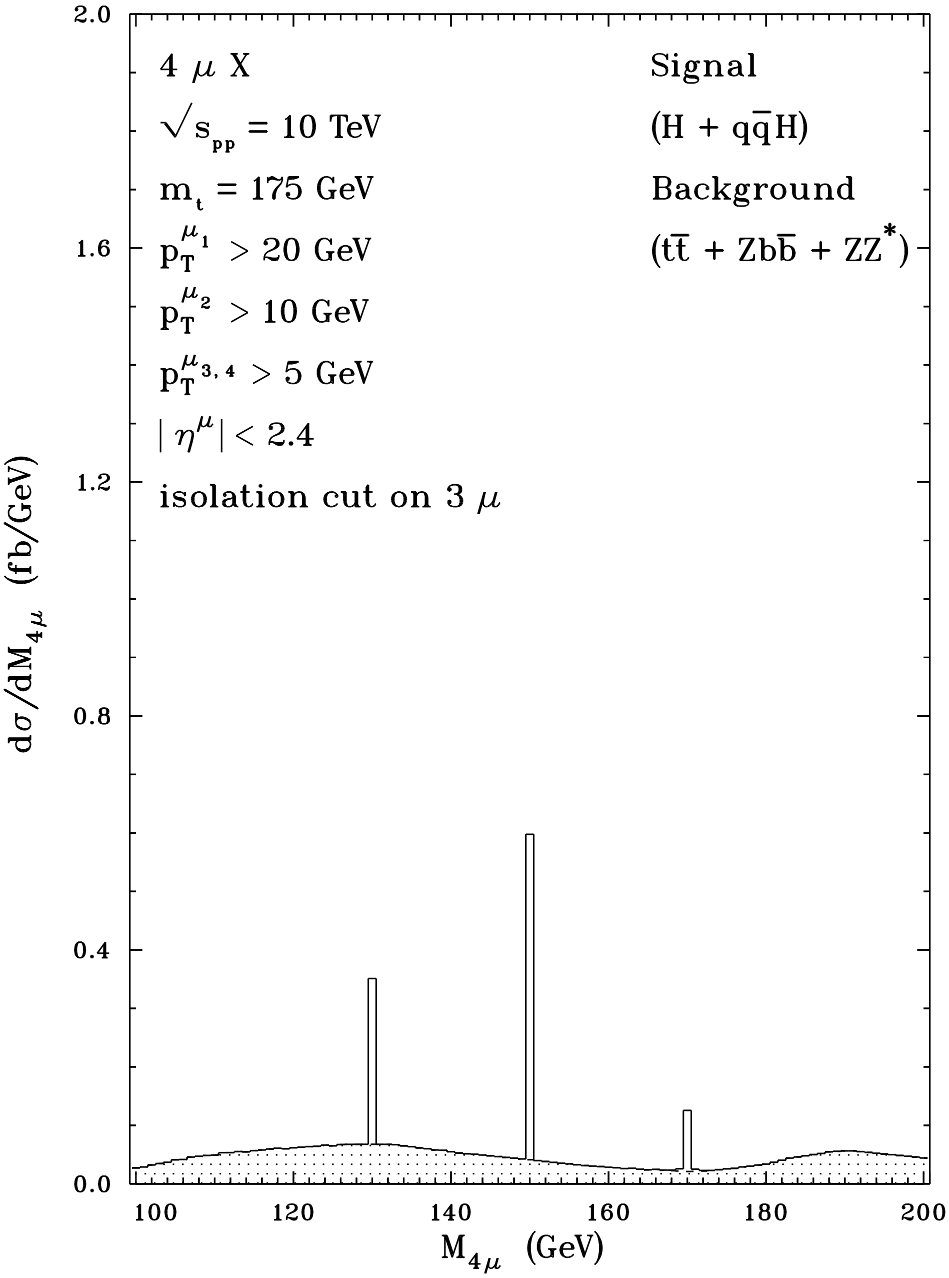
4 μ X
√s_pp = 10 TeV
m_t = 175 GeV
p_T^μ1 > 20 GeV
p_T^μ2 > 10 GeV
p_T^μ3,4 > 5 GeV
|η^μ| < 2.4
isolation cut on 3 μ
Signal
(H + qq̄H)
Background
(tt̄ + Zbb̄ + ZZ*)
dσ/dM_4μ (fb/GeV)
M_4μ (GeV)
2.0
1.6
1.2
0.8
0.4
0.0
100
120
140
160
180
200

Fig. 7

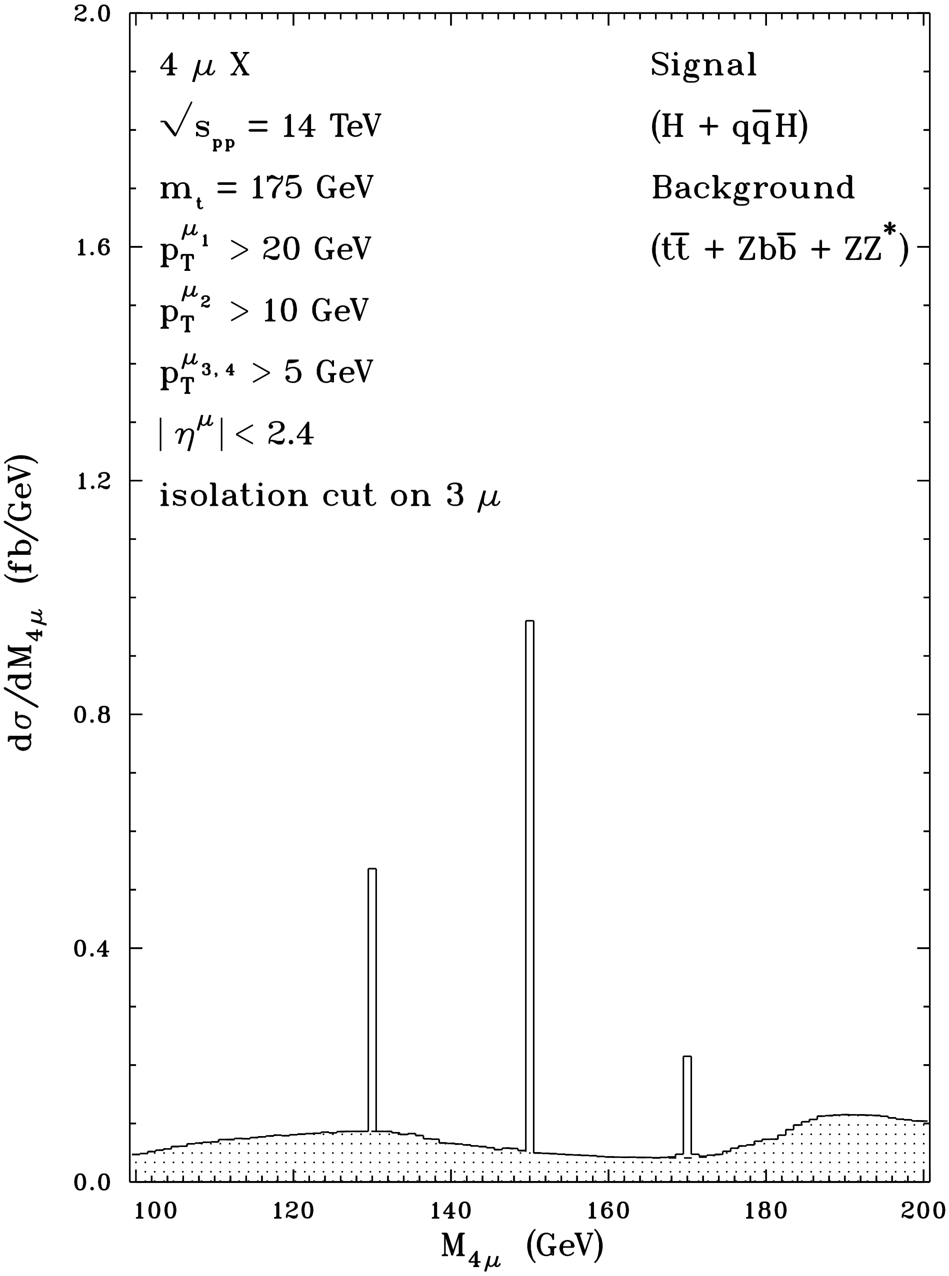

4 μ X
√s_pp = 14 TeV
m_t = 175 GeV
p_T^μ1 > 20 GeV
p_T^μ2 > 10 GeV
p_T^μ3,4 > 5 GeV
|η^μ| < 2.4
isolation cut on 3 μ
Signal
(H + qq̄H)
Background
(tt̄ + Zbb̄ + ZZ*)
dσ/dM_4μ (fb/GeV)
M_4μ (GeV)
2.0
1.6
1.2
0.8
0.4
0.0
100
120
140
160
180
200

Fig. 8

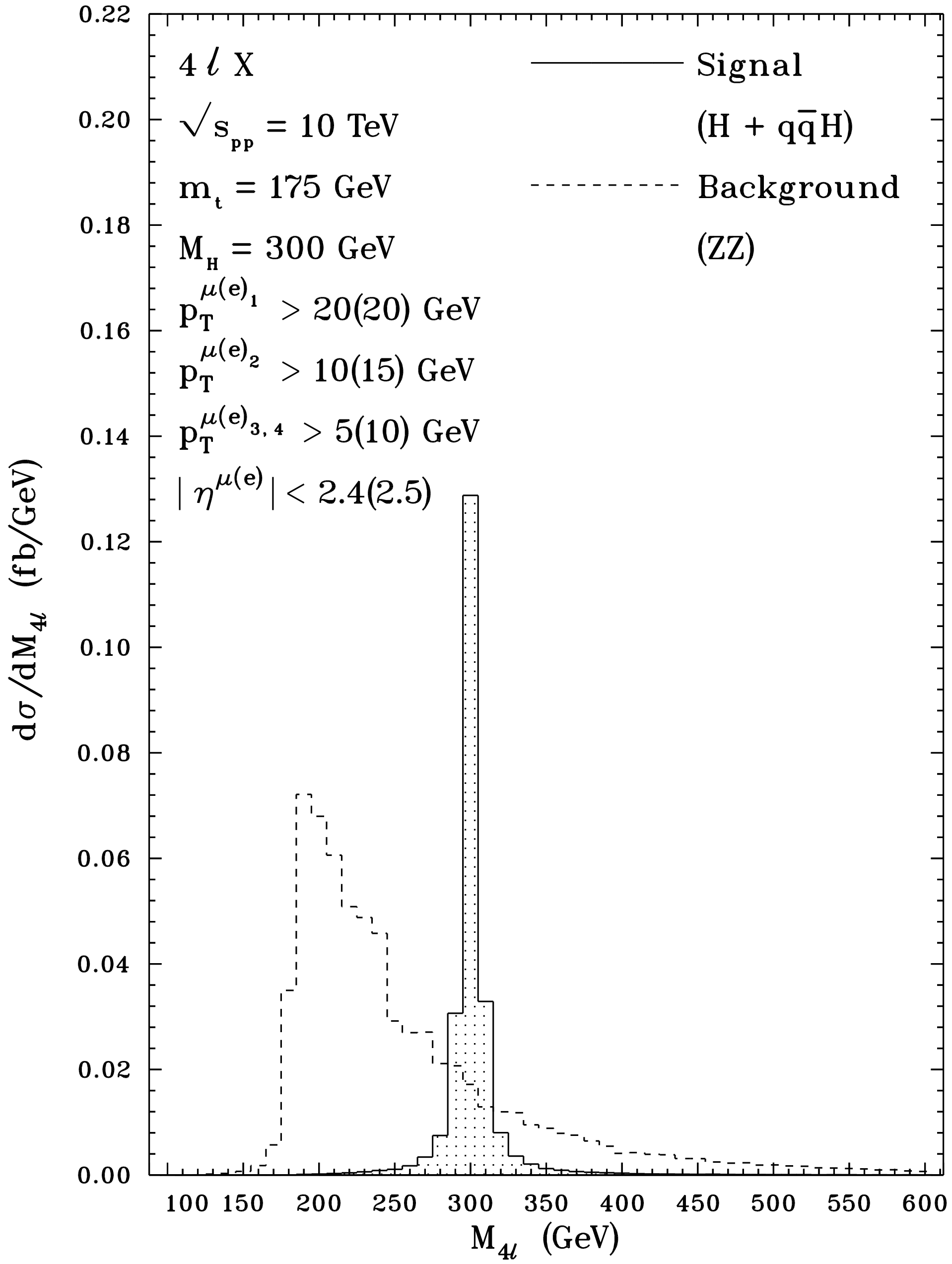

4 ℓ X
$\sqrt{s_{pp}}$ = 10 TeV
m_t = 175 GeV
M_H = 300 GeV
$p_T^{\mu(e)_1}$ > 20(20) GeV
$p_T^{\mu(e)_2}$ > 10(15) GeV
$p_T^{\mu(e)_{3,4}}$ > 5(10) GeV
$|\eta^{\mu(e)}|$ < 2.4(2.5)
Signal
(H + $q\bar{q}$H)
Background
(ZZ)
$d\sigma/dM_{4\ell}$ (fb/GeV)
$M_{4\ell}$ (GeV)
0.00
0.02
0.04
0.06
0.08
0.10
0.12
0.14
0.16
0.18
0.20
0.22
100
150
200
250
300
350
400
450
500
550
600

Fig. 9a

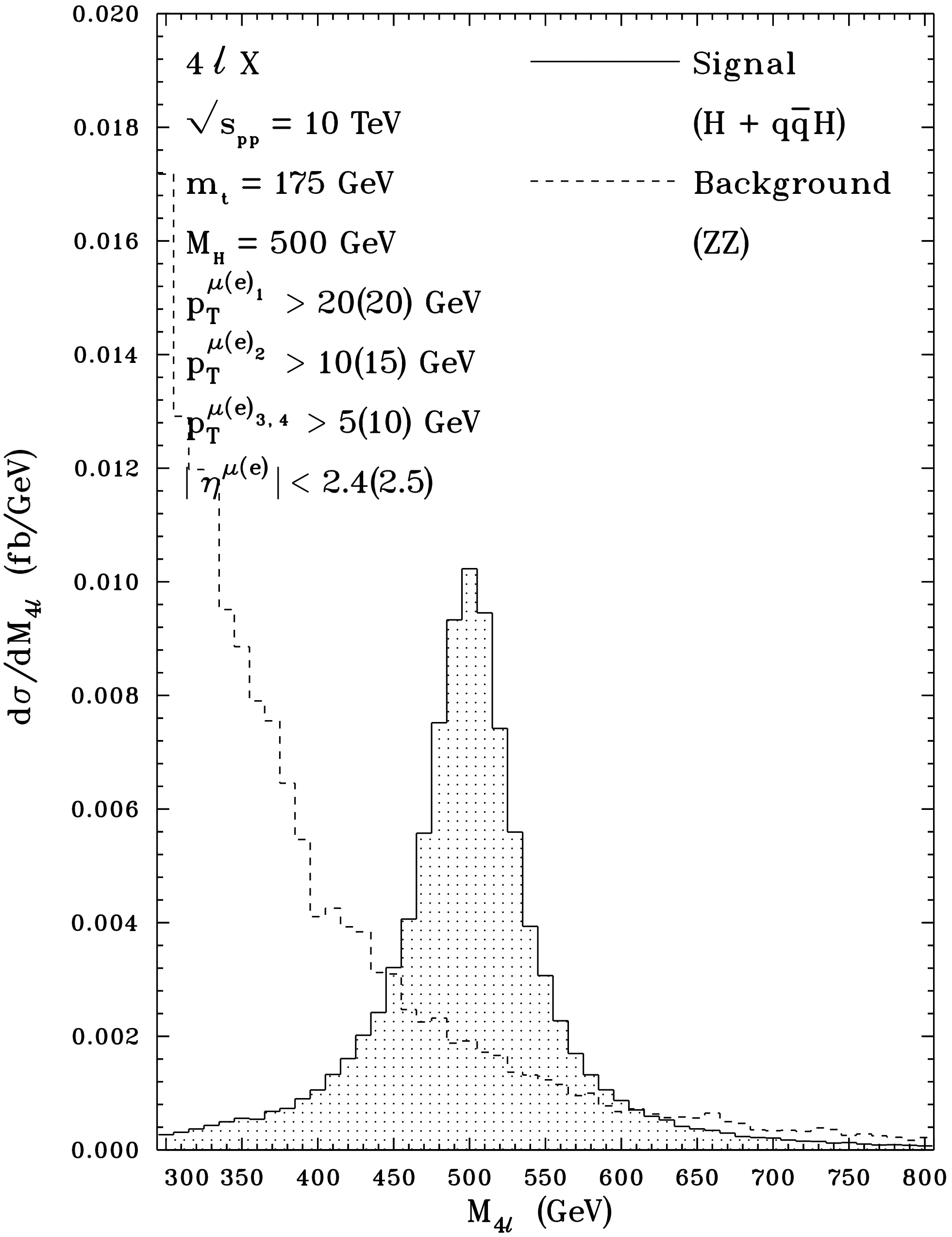

0.020
0.018
0.016
0.014
0.012
0.010
0.008
0.006
0.004
0.002
0.000
$d\sigma/dM_{4\ell}$ (fb/GeV)
300 350 400 450 500 550 600 650 700 750 800
$M_{4\ell}$ (GeV)
$4\,\ell\,X$
$\sqrt{s_{pp}} = 10$ TeV
$m_t = 175$ GeV
$M_H = 500$ GeV
$p_T^{\mu(e)_1} > 20(20)$ GeV
$p_T^{\mu(e)_2} > 10(15)$ GeV
$p_T^{\mu(e)_{3,4}} > 5(10)$ GeV
$|\eta^{\mu(e)}| < 2.4(2.5)$
Signal
$(H + q\bar{q}H)$
Background
(ZZ)

Fig. 9b

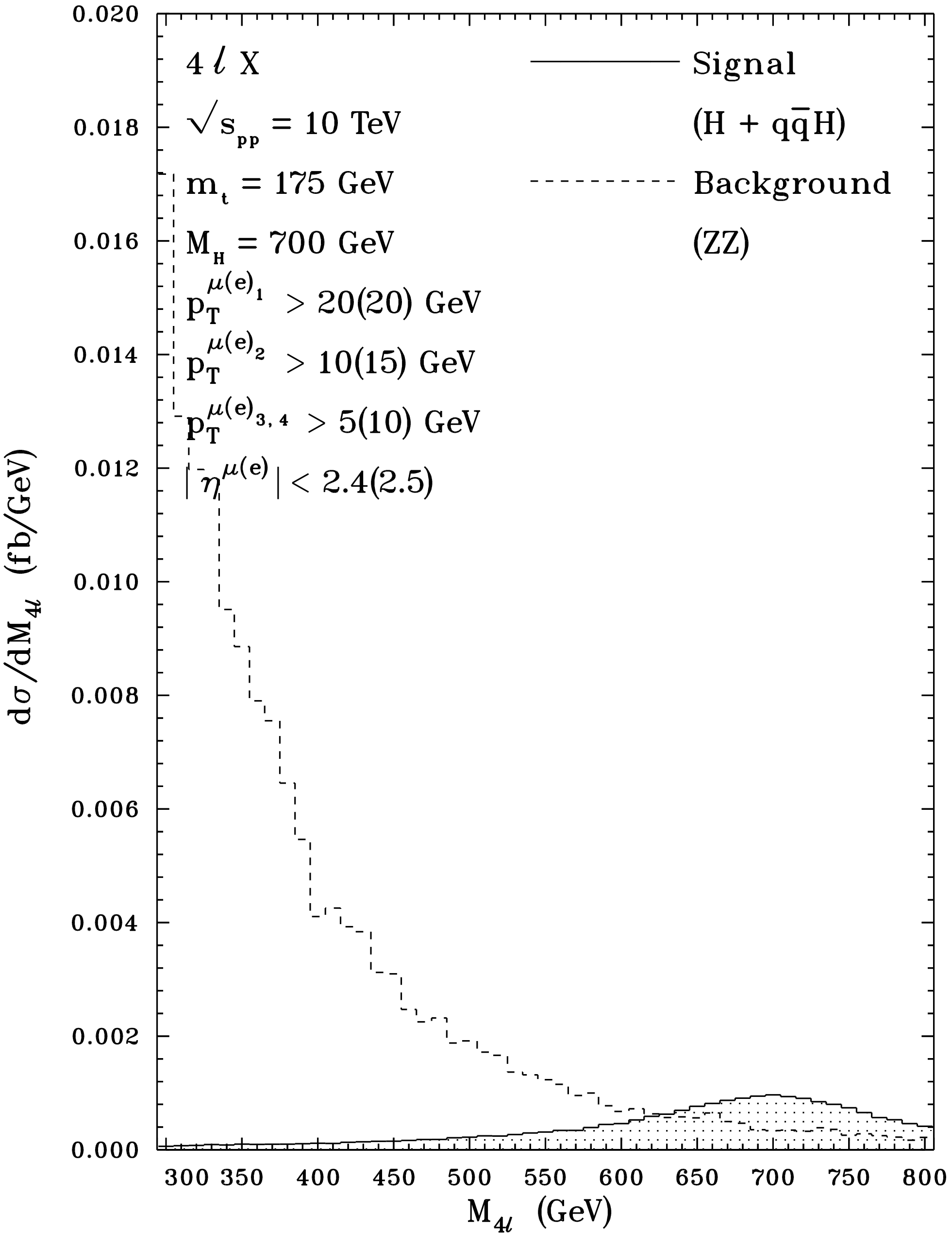

4 ℓ X
√s_pp = 10 TeV
m_t = 175 GeV
M_H = 700 GeV
p_T^μ(e)_1 > 20(20) GeV
p_T^μ(e)_2 > 10(15) GeV
p_T^μ(e)_3,4 > 5(10) GeV
|η^μ(e)| < 2.4(2.5)
Signal
(H + qq̄H)
Background
(ZZ)
dσ/dM_4ℓ (fb/GeV)
M_4ℓ (GeV)
0.020
0.018
0.016
0.014
0.012
0.010
0.008
0.006
0.004
0.002
0.000
300
350
400
450
500
550
600
650
700
750
800

Fig. 9c

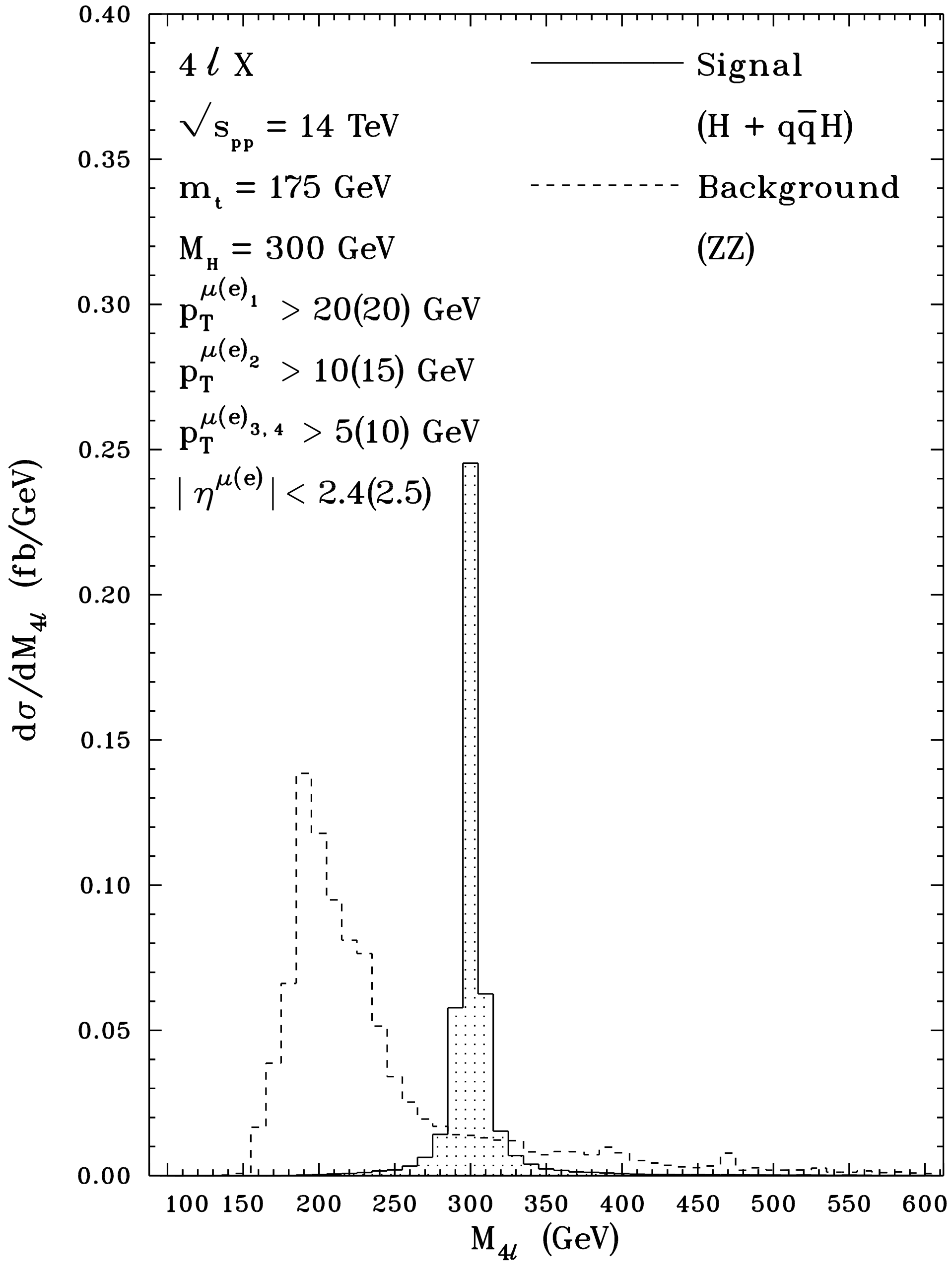

0.40
0.35
0.30
0.25
0.20
0.15
0.10
0.05
0.00
100 150 200 250 300 350 400 450 500 550 600
$M_{4\ell}$ (GeV)
$d\sigma/dM_{4\ell}$ (fb/GeV)
$4\,\ell$ X
$\sqrt{s_{pp}}$ = 14 TeV
m_t = 175 GeV
M_H = 300 GeV
$p_T^{\mu(e)_1} > 20(20)$ GeV
$p_T^{\mu(e)_2} > 10(15)$ GeV
$p_T^{\mu(e)_{3,4}} > 5(10)$ GeV
$|\eta^{\mu(e)}| < 2.4(2.5)$
Signal
$(H + q\bar{q}H)$
Background
(ZZ)

Fig. 10a

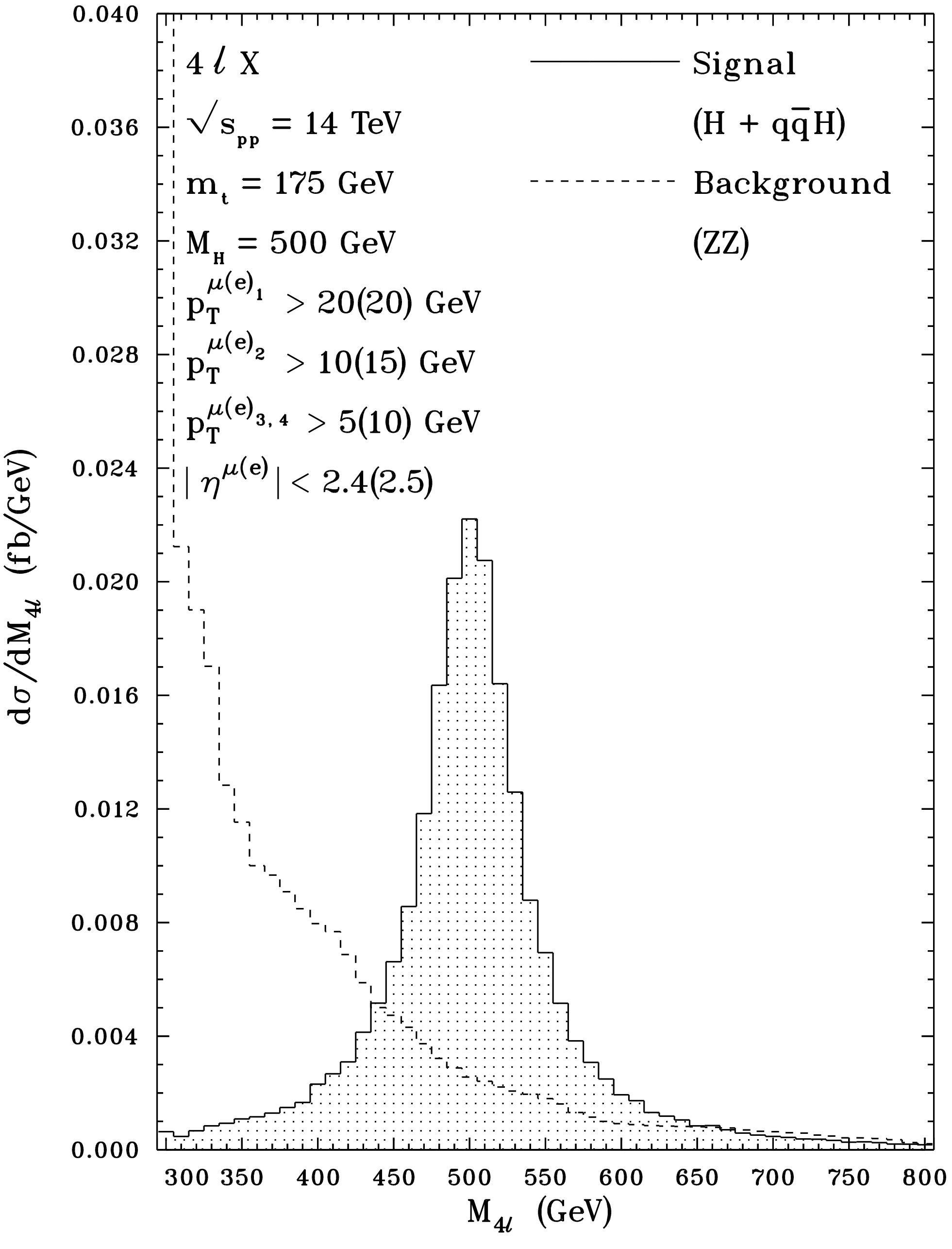

0.040
0.036
0.032
0.028
0.024
0.020
0.016
0.012
0.008
0.004
0.000
300 350 400 450 500 550 600 650 700 750 800
$M_{4\ell}$ (GeV)
$d\sigma/dM_{4\ell}$ (fb/GeV)
$4\ell X$
$\sqrt{s_{pp}}$ = 14 TeV
m_t = 175 GeV
M_H = 500 GeV
$p_T^{\mu(e)_1}$ > 20(20) GeV
$p_T^{\mu(e)_2}$ > 10(15) GeV
$p_T^{\mu(e)_{3,4}}$ > 5(10) GeV
$|\eta^{\mu(e)}| < 2.4(2.5)$
Signal
$(H + q\bar{q}H)$
Background
(ZZ)

Fig. 10b

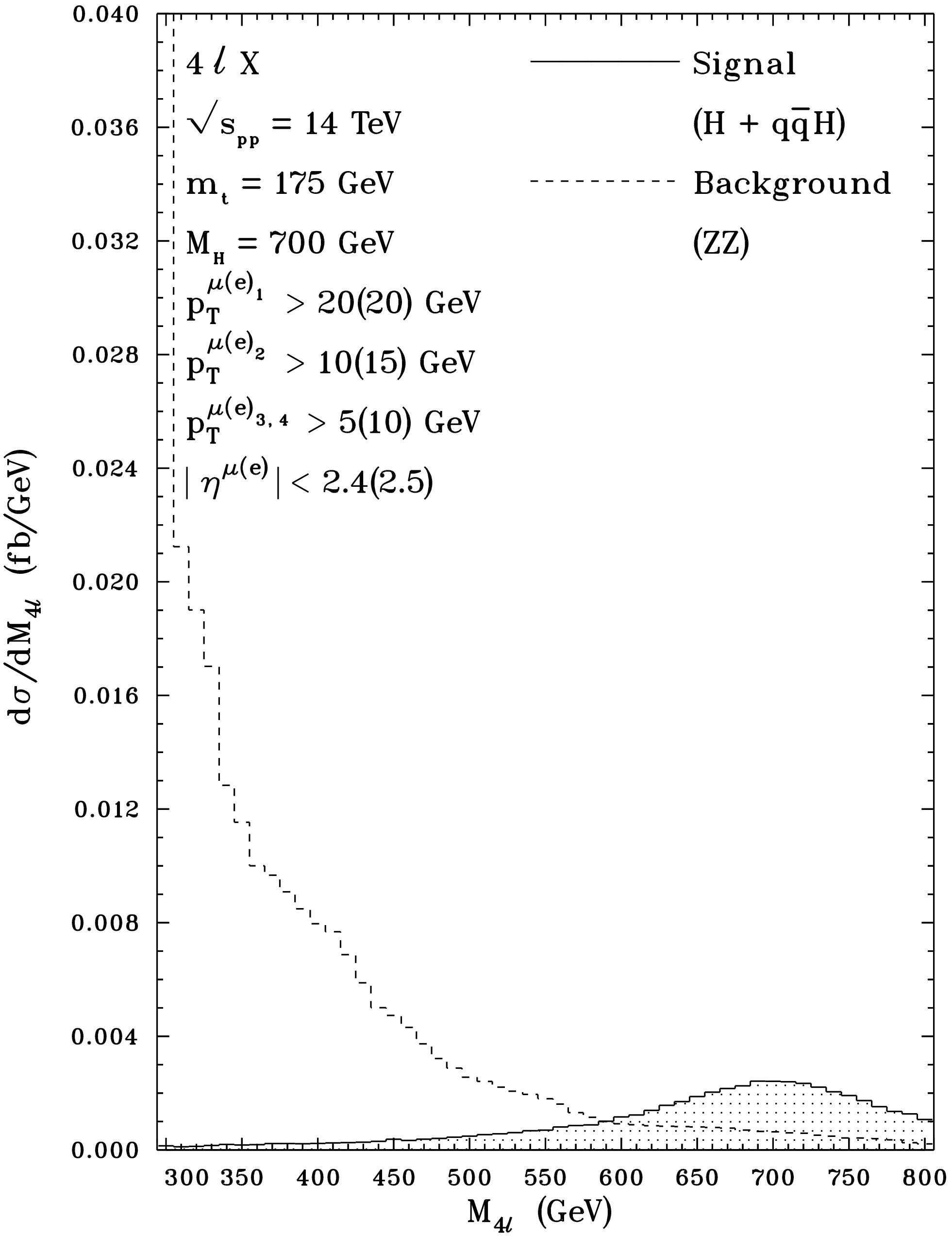

4 ℓ X
$\sqrt{s_{pp}}$ = 14 TeV
m_t = 175 GeV
M_H = 700 GeV
$p_T^{\mu(e)_1} > 20(20)$ GeV
$p_T^{\mu(e)_2} > 10(15)$ GeV
$p_T^{\mu(e)_{3,4}} > 5(10)$ GeV
$|\eta^{\mu(e)}| < 2.4(2.5)$
Signal
(H + q$\bar{q}$H)
Background
(ZZ)
$d\sigma/dM_{4\ell}$ (fb/GeV)
$M_{4\ell}$ (GeV)
0.040
0.036
0.032
0.028
0.024
0.020
0.016
0.012
0.008
0.004
0.000
300 350 400 450 500 550 600 650 700 750 800

Fig. 10c

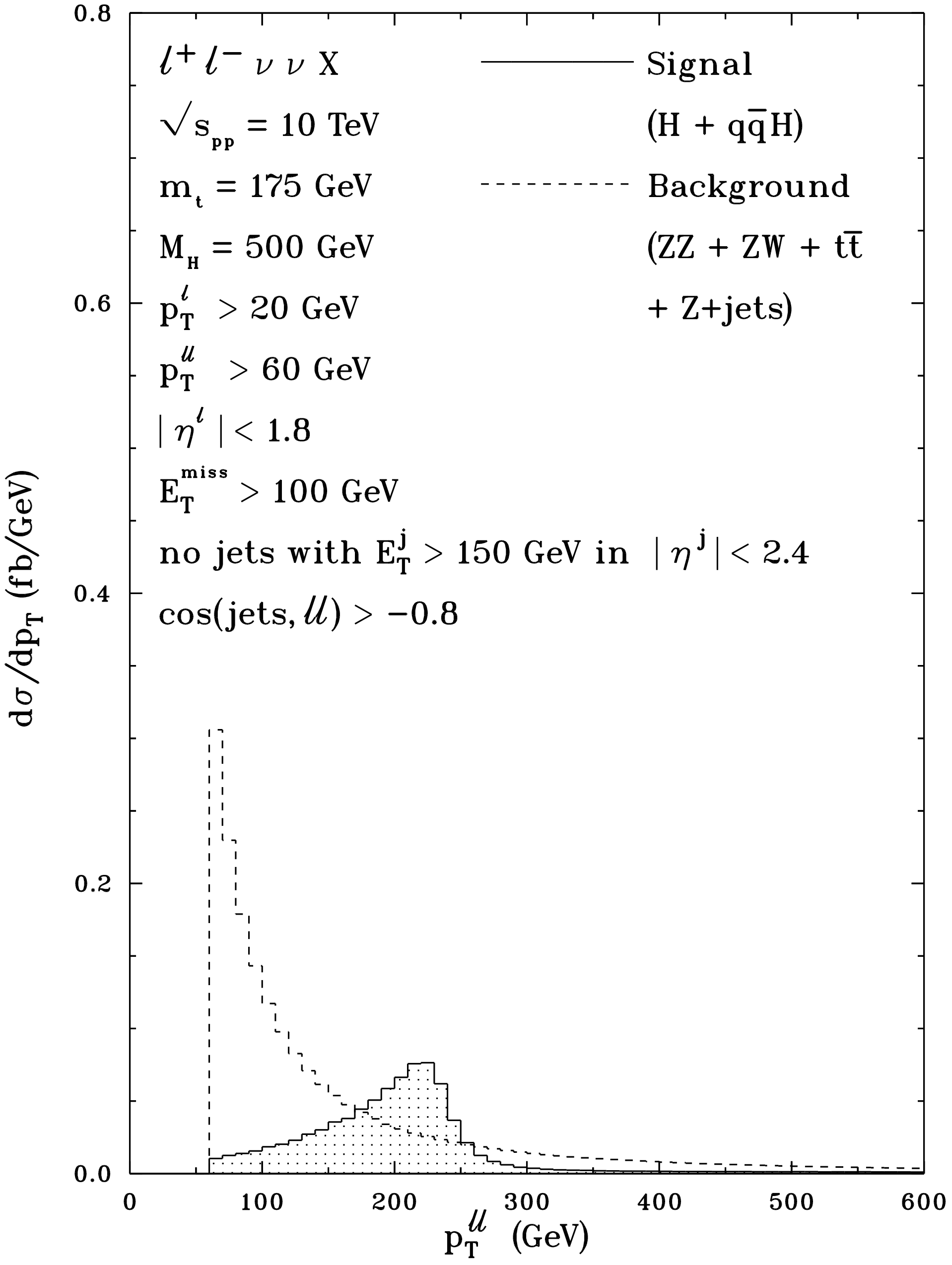
$\ell^+ \ell^- \nu \nu X$
$\sqrt{s_{pp}} = 10$ TeV
$m_t = 175$ GeV
$M_H = 500$ GeV
$p_T^\ell > 20$ GeV
$p_T^{\ell\ell} > 60$ GeV
$|\eta^\ell| < 1.8$
$E_T^{miss} > 100$ GeV
no jets with $E_T^j > 150$ GeV in $|\eta^j| < 2.4$
$\cos(\text{jets}, \ell\ell) > -0.8$
Signal
($H + q\bar{q}H$)
Background
($ZZ + ZW + t\bar{t}$
+ Z+jets)
$d\sigma/dp_T$ (fb/GeV)
$p_T^{\ell\ell}$ (GeV)
0.0
0.2
0.4
0.6
0.8
0
100
200
300
400
500
600

Fig. 11

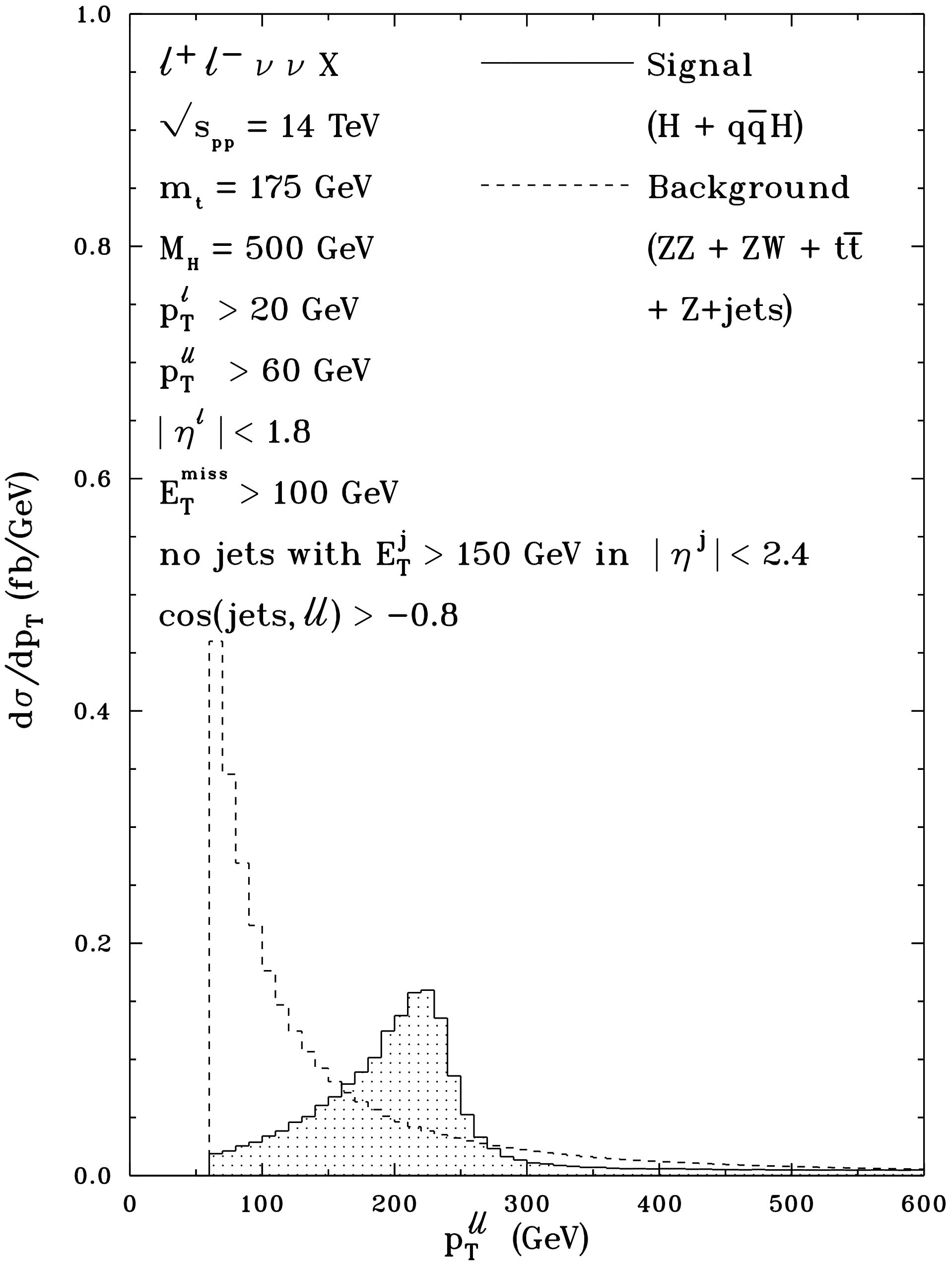

$\ell^+ \ell^- \nu \nu$ X
$\sqrt{s_{pp}}$ = 14 TeV
m_t = 175 GeV
M_H = 500 GeV
p_T^ℓ > 20 GeV
$p_T^{\ell\ell}$ > 60 GeV
$|\eta^\ell| < 1.8$
E_T^{miss} > 100 GeV
no jets with E_T^j > 150 GeV in $|\eta^j| < 2.4$
cos(jets, $\ell\ell$) > −0.8
Signal
(H + q$\bar{q}$H)
Background
(ZZ + ZW + t$\bar{t}$
+ Z+jets)
$d\sigma/dp_T$ (fb/GeV)
$p_T^{\ell\ell}$ (GeV)
0.0
0.2
0.4
0.6
0.8
1.0
0
100
200
300
400
500
600

Fig. 12